

Relativistic Laser-Matter Interaction and Relativistic Laboratory Astrophysics

S. V. Bulanov^{1,2}, T. Zh. Esirkepov¹, D. Habs^{3,4}, F. Pegoraro⁵, T. Tajima^{1,3,4}

¹Advanced Photon Research Center, JAEA, 8-1 Umemidai, Kizugawa, 619-0215 Kyoto, Japan

²A. M. Prokhorov Institute of General Physics, RAS, Vavilov street, 38, 119991 Moscow, Russia

³Sektion Physik, Ludwig-Maximilians-Universitaet Muenchen, D-85748 Garching, Germany

⁴Max-Planck-Institut fuer Quantenoptik, D-857748 Garching, Germany

⁵Physics Dept. and CNISM, University of Pisa, Largo Pontecorvo, 3, 56127 Pisa, Italy

Abstract

The paper is devoted to the prospects of using the laser radiation interaction with plasmas in the laboratory relativistic astrophysics context. We discuss the dimensionless parameters characterizing the processes in the laser and astrophysical plasmas and emphasize a similarity between the laser and astrophysical plasmas in the ultrarelativistic energy limit. In particular, we address basic mechanisms of the charged particle acceleration, the collisionless shock wave and magnetic reconnection and vortex dynamics properties relevant to the problem of ultrarelativistic particle acceleration.

PACS numbers: 52.27.Ny, 52.72.+v

Contents

I. Introduction	4
II. Dimensionless Parameters that Characterize the Interaction Regimes of High Intensity Electromagnetic Waves with Matter	7
A. Principle of Qualitative Scaling	7
B. Parameters of Strong EMW Propagating in Plasmas	8
C. Interaction of EMW with Plasmas in the Radiation-Dominated Regime	12
D. Probing Nonlinear Vacuum	13
E. EMW Parameters under Space Plasma Conditions	16
III. Acceleration of Charged Particles in the EMW Interaction with Plasmas	18
A. Electron Accelerator	18
B. Ion Accelerator	22
1. Ion acceleration during plasma expansion into vacuum	23
2. Radiation pressure dominated regime of the ion acceleration	24
IV. Mini-black-holes on Earth	27
V. Flying Mirror Concept of the Electromagnetic Wave Intensification	29
VI. Reconnection of Magnetic Field Lines & Vortex Patterns	32
A. Dimensionless parameters describing the relative roles of nonlinear, dissipative and Hall effects	32
B. Current Sheet	34
C. Magnetic Reconnection in Collisionless Plasmas	35
D. Charged Particle Acceleration	37
E. Electron Vortices in Collisionless Plasmas	38
F. A Role of the Weibel Instability in the Quasistatic and Turbulent Magnetic Field Generation	41
VII. Relativistic Rotator	42
VIII. Shock Waves	43

A. Shock Waves in Supernova Remnants	44
B. Collisionless Shock Waves	46
C. Diffusive Acceleration of Charged Particles at the Shock Wave Front	47
IX. Conclusions	50
Acknowledgement	50
References	50

I. INTRODUCTION

High-power laser facilities have made unprecedented progress in recent years and the nearest future their radiation may reach intensities of $10^{24}\text{W}/\text{cm}^2$ and higher [1]. As a result of laser technology progress the laser-matter interaction entered regimes of interest for astrophysics. Typically in the course of laser irradiation of targets shock waves are generated; the target compression is accompanied by the Rayleigh-Taylor (RT) and Richtmayer-Meshkov (RM) instability development; collimated plasma jets are observed; the matter equation of state (EOS) acquires new properties under extreme pressure, density and temperature conditions; the laser plasma emits high energy charged particle beams and high- and low-frequency powerful electromagnetic radiation. Gathering of these facts principal for both space and laboratory physics has initiated works in the so-called laboratory astrophysics [2] with the aim to model the processes of key importance for the space objects under laboratory conditions. Concerning the laser facilities, the present day laser systems can be subdivided into two categories. The first category includes lasers with a relatively long pulse of pico- and nanosecond duration and generally low repetition rate. These high energy and power laser facilities have been mainly developed for purposes of inertial confinement fusion with the laser pulse and target parameters corresponding to the collisional hydrodynamics phenomena [3]. In context of laboratory astrophysics they are used for experiments on shock waves, including the radiative shocks and RT&RM instability, the jet formation, and the EOS studies. The second category includes table top size lasers, whose pulse duration is of the order of a few tens of a femto-second with high repetition rate [4]. Due to ultra short pulse duration and high contrast, these relatively moderate energy lasers can produce extremely high power and relativistically high intensity electromagnetic pulses. However, the role of both kinds of laser systems is complementary for the development of experimental facilities for the purposes of relativistic laboratory astrophysics.

Generic questions for astrophysics such as whether we are living in the Universe or in the Multiverse [5], related discussions of the inflation era in the Multiverse evolution [6] and probing our world's dimensions are related to quantum gravitation physics and deal with the observational cosmology, in particular with an analysis of the cosmic black body radiation, the nuclear synthesis and Type I supernovae radiation (see [7]), are yet out of the energy range accessible with present day lasers. The quantum gravitation energy scale is given by

the Planck energy, $\sqrt{\hbar c^3/G} \approx 10^{19}\text{GeV}$, which corresponds to the mass $\sqrt{\hbar c/G} \approx 10^{-5}\text{g}$ and the length $\sqrt{\hbar G/c^3} \approx 10^{-33}\text{ cm}$. In quantum field theory the unification energy scale corresponds to 10^{16}GeV [8, 9]. These energy frontiers are yet well above of nowadays laser pulse energies. Fortunately, new physics such as the Higgs boson detection and exploration of the physics beyond the Standard Model is anticipated to be met at a substantially lower energy level in the range of several TeV in the experiments planned with the Large Hadron Collider (LHC), as summarized in Ref. [9]. If relativistic laser plasmas can provide the charged particle acceleration up to the TeV energy level, laser accelerators will make a considerable impact to high energy physics, to finding answers on black hole and brane production under the terrestrial conditions [10], to test causality [11] and to study the quark-gluon plasmas [12].

We may see that the main field of studies of astrophysical phenomena with high power lasers lies in the electrodynamics of continuous media in the relativistic regime [13]. Since matter irradiated by ultrastrong electromagnetic waves (EMW) is ionized during a time interval comparable with the wave period and becomes a plasma and under astrophysical conditions approximately 95% of barionic part of matter is in the plasma state, the object of our studies is the relativistic laser and astrophysical plasma.

If we address to the problems of contemporary relativistic astrophysics, first of all questions on the mechanisms of the cosmic ray acceleration and on the properties of strong EMW interaction with relativistic plasmas attract our attention [14]. In space plasmas basic mechanisms of charged particle acceleration are connected with the reconnection of magnetic field lines, which is accompanied by the strong and regular electric field generation (it occurs in the planet magnetospheres, in binary stellar systems, in accretion disks, in the magnetar magnetospheres, etc.) and with collisionless shock waves, at the fronts of which the charged particle acceleration occurs (this happens in interplanetary space, during supernova explosions, in colliding galaxies, etc.) [14, 15].

The laser accelerator development relies upon the fact that under the terrestrial laboratory conditions presently one of the most powerful sources of coherent electromagnetic radiation is provided by lasers [13]. Wakefield accelerators, [16] and [17], presently provide the most advanced schemes for electron acceleration and they may be suggested to be good candidates for the charged particle acceleration in space [14, 18]. One of the efficient mechanisms of ion acceleration in laser plasmas utilizes the radiation pressure of electromagnetic

waves interacting with plasmas (see Refs. [19] and [20]). Radiation pressure is a very effective mechanism of momentum transfer to charged particles. This mechanism was introduced long ago [21] and physical conditions of interest range from stellar structures and radiation generated winds (see e.g. Refs. [22]), to the formation of “photon bubbles” in very hot stars and accretion disks [23], to particle acceleration in the laboratory [19, 24, 25], see in addition Refs. [26, 27], and in high energy astrophysical environments [28].

Utilization of the plasma nonlinear properties for the electromagnetic wave intensification can result in much higher intensity and power. In this case a fundamental role is played by relativistic mirrors, which are thin electron sheets induced by the laser radiation moving with a speed close to the speed of light in vacuum, as proposed in Ref. [29]. We note the fruitfulness of the relativistic mirror concept for solving a wide range of problems in modern theoretical physics. Relativistic mirrors are important elements in the theory of the dynamical Casimir effect [30], with regard to the Unruh radiation [31] and other nonlinear vacuum phenomena [32, 33, 34, 36, 37]. Relativistic mirrors made by wake waves may lead to an electromagnetic wave intensification resulting in an increase of pulse power up to the level when the electric field of the wave reaches the Schwinger limit [38] when electron-positron pairs are created from the vacuum and the vacuum refractive index becomes nonlinearly dependent on the electromagnetic field strength. In quantum field theory particle creation from the vacuum attracts a great attention, because it provides a typical example of non perturbative processes [39]. Nonlinear QED vacuum properties can in future be probed with such strong and powerful electromagnetic pulses.

If we trace a relationship between astrophysics and laser physics, we can see a number of publications devoted to the laboratory modeling of astrophysical processes [2]. As known there has been an interest in modeling space physics with laboratory experiments for many years. The first modeling of processes fundamental for space physics in terrestrial laboratories has been done by Kristian Birkeland, who more than 100 years ago conducted first experiments on studying the auroral regions in the earth magnetosphere [40]. Later on progress has been achieved in the laboratory modeling of various processes [41, 42], including the magnetic field reconnection [43], collisionless shock waves [44], which provide mechanisms for charged particle acceleration under various astrophysical conditions (see Ref. [14]).

In the present paper we address plasma processes relevant to space physics, which occur

in the relativistic and collisionless regimes.

II. DIMENSIONLESS PARAMETERS THAT CHARACTERIZE THE INTERACTION REGIMES OF HIGH INTENSITY ELECTROMAGNETIC WAVES WITH MATTER

A. Principle of Qualitative Scaling

Laboratory experiments for studying astrophysical phenomena are of two types [48]. The first type of experiments can be referred to as *configuration modeling*, which is aiming at simulating the actual configuration of a system, e.g. the whole Earth's magnetosphere (for example see Ref. [45], where the results of the laser-plasma experiments on the simulation of the global impact of the coronal mass ejections onto the Earth's magnetosphere are presented). The second type of experiments corresponds to *process simulation*, i. e. they are aiming at studying the properties of physical processes relevant to astrophysical phenomena [2]. There are a number of nonlinear plasma physical processes that require their clarification.

Physical systems obey scaling laws, which can also be presented as similarity rules. In the theory of similarity and modeling the key role is played by dimensionless parameters that characterize the phenomena under consideration [46]. The principle requirement of the laboratory modeling is the equality of the key dimensionless parameters in the modeled processes. In cases of modeling astrophysical phenomena where this equality can hardly be respected, instead the *principle of limited similarity* (PLS) or *principle of qualitative scaling* has been formulated in Refs. [47] and [48]. According to the PLS those dimensionless parameters, which are relevant in a certain context and which are much larger or smaller than unity under astrophysical conditions must retain this property (i.e. be much larger or smaller than unity) in the laboratory experiments modeling the astrophysical process. Below we present the key dimensionless parameters that characterize the high intensity electromagnetic wave (EMW) interaction with matter (see also Refs. [49, 50]).

B. Parameters of Strong EMW Propagating in Plasmas

The intensity of an electromagnetic wave pulse is defined by its electric field amplitude through the expression: $I = cE_0^2/4\pi$, which is related to the Poynting vector

$$P = \frac{c}{4\pi} [E \times B]. \quad (1)$$

The power of the EMW is equal to the integral over its transverse cross-section S ,

$$P = \frac{c}{4\pi} \oint_S ([E \times B] \cdot n) dS = I S. \quad (2)$$

The time integral of the power gives the pulse energy, $\mathcal{E} = \mathcal{P}\tau_p$, where τ_p , is the pulse duration. Other important parameters are the pulse frequency, ω_0 , which is related to its wavelength, $\lambda_0 = 2\pi c/\omega_0$, and the pulse polarization.

The first of the dimensionless parameters which characterizes the EMW packet is the ratio of the pulse length, $l_p = c\tau_p$, to the radiation wavelength, λ_0 . We shall denote this ratio as $N_p = l_p/\lambda_0$. It is equal to the number of wavelengths per pulse, and is Lorentz invariant.

If the EMW intensity is relatively low, irradiated matter is not ionized. We notice that the typical energy of a photon in the laser parameter range with wavelengths in the micron range is of the order of one electron-volt and is substantially smaller than the binding energy of an electron inside an atom, $\hbar\omega_0 \ll W_b$, i.e. it is smaller than the atomic ionization potential. In this case the characteristic dimensionless parameter of the interaction is the ratio between the amplitude of the electric field in the laser pulse, $E = \sqrt{4\pi I/c}$, and the atomic electric field, E_a . The latter is equal to the electric field of the proton at a distance of a Bohr radius, $a_B = \hbar^2/m_e e^2 \simeq 5.3 \times 10^{-9} \text{cm}$, i.e. $E_a = e/a_B^2 = m_e^2 e^5/\hbar^4$. The electron binding energy is $W_b = \hbar^2/2a_B^2 m_e$ and it corresponds to the frequency $\omega_a = W_b/\hbar$. The above condition, $\hbar\omega_0 \ll W_b$, is equivalent to the inequality $\hbar\omega_0/W_b = \omega_0/\omega_a \ll 1$. The dimensionless parameter

$$\frac{E_0}{E_a} = \frac{\hbar^4 E_0}{m_e^2 e^5} \quad (3)$$

becomes equal to unity for a laser radiation intensity equal to $m_e^4 e^{10} c/4\pi \hbar^8 \simeq 10^{16} \text{ W/cm}^2$. For small but finite values of this parameter, i.e. in the limit $I < 10^{16} \text{ W/cm}^2$, the atom is not ionized, unless the multiphoton processes come into play, the EMW-matter interaction can be described within the framework of perturbation theory. When the parameter E_0/E_a approaches unity, the potential inside the atom changes its form and the so-called tunnel

ionization becomes possible. The tunnel ionization probability is given by the Keldysh formula [51]

$$w = \omega_a \exp \left[-\frac{2W_b}{\hbar\omega_0} f(\gamma_K) \right], \quad (4)$$

where the function $f(\gamma_K) \approx 2\gamma_K/3$ for $\gamma_K \ll 1$ and $f(\gamma_K) \approx \ln 2\gamma_K - 1/2$ for $\gamma_K \gg 1$. The adiabatic parameter γ_K is defined as

$$\gamma_K = \omega_0 \frac{\sqrt{2m_e W_b}}{eE_0} = \sqrt{\frac{2\hbar\omega_a}{a_0^2 m_e c^2}}. \quad (5)$$

Here introduced is the EMW dimensionless amplitude,

$$a_0 = \frac{eE_0}{m_e \omega_0 c}. \quad (6)$$

In the limit $\gamma_K \ll 1$, i.e. for a relatively strong electromagnetic wave, Eq. (4) corresponds to the ionization probability by a constant electric field,

$$w = 2\omega_a \frac{E_a}{E_0} \exp \left(-\frac{2E_a}{3E_0} \right). \quad (7)$$

For intensities larger than $m_e^4 e^{10} c / 4\pi \hbar^8 \simeq 10^{16}$ W/cm² the deformation of the potential inside the atoms caused by the laser pulse field becomes so strong that the electron energy level becomes larger than the maximum value of the potential. As a result, the electron appears as if in a free state and leaves the atom. Due to the periodicity of the electric field, there is a probability that the electron will return after a half of the wave period. Recollisions with the ions lead to the generation of high order harmonics [52]. However, for a very strong electromagnetic wave the effects of the wave magnetic field decrease this probability. In this case the matter becomes ionized in one optical period and plasma processes start to play a key role.

Under the action of the electromagnetic wave the plasma electrons oscillate at the wave frequency. In the limit $v \ll c$ their quiver velocity is approximately equal to $v_E = eE_0/m_e \omega_0$. In the non-relativistic limit, when $v_E/c \ll 1$ or $a_0 \ll 1$, the electron quiver amplitude is smaller than the laser wavelength, λ_0 . Under the action of the electromagnetic wave, given by the vector potential $A_\perp(x - ct)$, the electrons oscillate at the wave frequency. From the equations of the motion we obtain that the transverse component of the generalized momentum $p_\perp - eA_\perp(x - ct)/c$ is constant. The particle energy and the longitudinal momentum component are related as [53]

$$\sqrt{m_e^2 c^4 + p_\perp^2 + p_\parallel^2} - p_\parallel c = h. \quad (8)$$

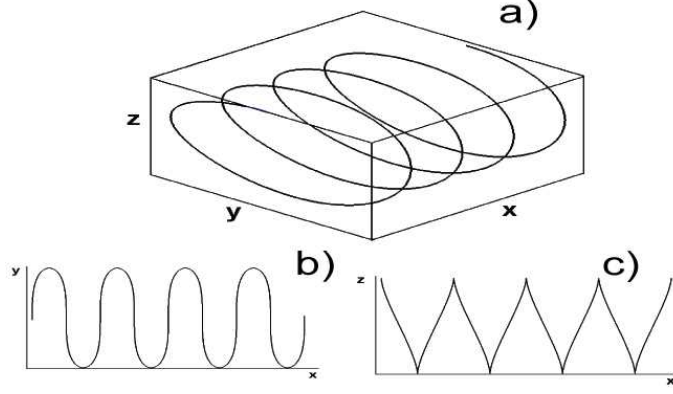


FIG. 1: Projectories of the charged particle trajectory, when it interacts with the elliptically polarized EMW.

In the reference frame where the particle was at rest before interaction with the laser pulse, the particle kinetic energy

$$K = m_e c^2 \left(\sqrt{1 + (p/m_e c)^2} - 1 \right) \quad (9)$$

and momentum $\mathbf{p} = (p_{\parallel}, p_{\perp})$ are given by expressions $K = m_e c^2 |a_{\perp}|^2 / 2$, $p_{\perp} = m_e c a_{\perp}$, $p_{\parallel} = m_e c |a_{\perp}|^2 / 2$. Here $a_{\perp} = e A_{\perp}(x - ct) / m_e c^2$. For $|a_{\perp}| > 1$ the particle acquires a relativistic energy, and the longitudinal component of its momentum is larger than the transverse component. Fig. 1 shows a typical trajectory of the charged particle in the electromagnetic wave.

The EMW behavior in a plasma differs from its behavior in vacuum, and depends on the electron density. In a plasma with a density n , a displacement of the electrons with respect to the ions generates the electric field. Its ratio to the laser electric field is $E/E_0 = 4\pi n e^2 / m_e \omega_0^2 = (\omega_{pe} / \omega_0)^2 = n / n_{cr}$, where $\omega_{pe} = \sqrt{4\pi n e^2 / m_e}$ is the Langmuir frequency and $n_{cr} = m_e \omega_0^2 / 4\pi e^2$ is the critical density. The dimensionless parameter

$$\frac{\omega_{pe}}{\omega_0} = \sqrt{\frac{n}{n_{cr}}} = \sqrt{\frac{4\pi n e^2}{m_e \omega_0^2}} \quad (10)$$

is a measure of the plasma collective response to a periodic electromagnetic field.

When an EMW propagates through a plasma, its group velocity, $v_g = \partial\omega / \partial k$, and phase velocity, $v_{ph} = \omega / k$, are not equal to each other and are related as $v_g v_{ph} = c^2$. While in vacuum the dispersion equation for the frequency, ω , and wave vector, k , takes the form $\omega^2 = k^2 c^2$, in a plasma it becomes $\omega^2 = k^2 c^2 + \omega_{pe}^2$. This dispersion equation can be

rewritten as $k = \sqrt{\omega^2 - \omega_{pe}^2}/c$, which shows that an EMW with a frequency below the Langmuir frequency cannot propagate through the plasma and that the electromagnetic field evanescence length in a high density plasma is of the order of the collisionless skin depth, $d_e = c/\omega_{pe}$, i.e. an overdense plasma with the electron density higher than the critical density is not transparent.

The collective response of the plasma, in addition to the transverse electromagnetic mode, exhibits longitudinal plasma oscillations, i.e., Langmuir waves. The electric field in a Langmuir wave oscillates with frequency $\omega = \omega_{pe}$. The group velocity of the Langmuir waves vanishes, $v_g = \partial\omega_{pe}/\partial k = 0$, and their phase velocity is determined by the wave number.

Relativistic effects change the dispersion equation due to the dependence of the Langmuir frequency on the wave amplitude. As found in Ref. [54], the frequency of a longitudinal wave depends on its amplitude $a_L = eE/m_e\omega_{pe}c$ as $\omega \approx \omega_{pe}(1 - 3a_L^2/4)$ for $a_L \ll 1$ and as $\omega \approx \omega_{pe}/\sqrt{8a_L}$ in the case $a_L \gg 1$.

For a circularly polarized electromagnetic wave the dispersion equation takes the form:

$$\omega^2 = k^2 c^2 + \frac{\omega_{pe}^2}{\sqrt{1 + a_0^2}}. \quad (11)$$

We see that the effective critical density increases as the EMW amplitude grows, i.e., the plasma is more transparent to high intensity electromagnetic radiation.

Large amplitude, finite length pulses of electromagnetic and Langmuir waves do not propagate independently since they are coupled by nonlinear processes. The Langmuir wave that is generated by an ultra short laser pulse, being left behind in the plasma and thus called the wake wave. It is of special interest since the structure of the electric field of this wake wave is favorable for charged particle acceleration. In a low density plasma the phase velocity of the wake wave can be very close to the speed of light in vacuum. In analogy to linear accelerators that use electric fields in the radio-frequency range in Ref. [16] it was proposed to use the wake field for charged particle acceleration.

The dimensionless amplitude, Eq. (6), is equal to the electron quiver momentum normalized to $m_e c$. For a pulse with an intensity corresponding to $a_0 > 1$, relativistic effects must be taken into account. The intensity of a linearly polarized electromagnetic wave can be written via a_0 as

$$I_L = \frac{\pi}{2} \frac{a_0^2}{\lambda_0^2} \frac{m_e c^3}{r_e} \approx 1.37 \times 10^{18} \times a_0^2 \times \left(\frac{1\mu m}{\lambda_0} \right)^2 \frac{W}{cm^2}. \quad (12)$$

If the wave is focused into a one wavelength spot, this intensity corresponds to the power $\mathcal{P} = a_0^2 \times 43 \text{ GW}$. At present laser intensities have reached a level above 10^{22} W/cm^2 [55].

When the electron energy approaches $3m_e c^2$, electron-positron pairs are generated during electron-nuclei collisions, [39]. The cross section of this process is given by

$$\sigma_{\pm} = \frac{28}{27\pi} r_e^2 (\alpha Z)^2 \left[\ln \left(\sqrt{1 + \left(\frac{p}{m_e c} \right)^2} \right) \right]. \quad (13)$$

Here Ze is the nucleus electric charge and $\alpha = e^2/\hbar c = 1/137$ is the fine-structure constant. Positron generation in a plasma has been discussed in a number of publications (e.g. see [56]) and was observed in the terawatt laser plasma interaction experiments [58]. We note a discussion of the pion and muon production in electron-positron and gamma plasmas [57].

C. Interaction of EMW with Plasmas in the Radiation-Dominated Regime

The dimensionless parameters characterizing the electromagnetic emission by an electron are the ratio between the classical electron radius and the electromagnetic wavelength, $r_e/\lambda_0 = e^2\omega_0/2\pi m_e c^3$, and the ratio between the photon energy and the electron rest mass energy, $\hbar\omega_0/m_e c^2$.

When an electron moves under the action of the electric and magnetic field of a wave, it emits electromagnetic radiation. The intensity of this radiation is given by the formula $W = (2e^2/3m_e^2 c^3)(dp_\mu/d\tau)^2$, where p_μ is the particle 4-momentum and τ is its proper time. When an ultrarelativistic charged particle moves along a circular trajectory in a circularly polarized electromagnetic wave, the radiation intensity is $W = (4\pi r_e/3\lambda_0)\omega_0 m_e c^2 a_0^4$. We see that the relative role of the radiation damping force is determined by the dimensionless parameter ε_{rad} , which is equal to

$$\varepsilon_{rad} = \frac{4\pi r_e}{3\lambda_0}. \quad (14)$$

By comparing the energy radiated by the particle per unit of time with the maximum energy gain in the electromagnetic wave $\partial_t \mathcal{E} = \omega_0 m_e c^2 a_0$, we obtain that the radiation effects become dominant at $a_0 \geq a_{rad} = \varepsilon_{rad}^{-1/3}$, i. e. in the limit $I > 10^{23} \text{ W/cm}^2$ for $1 \mu\text{m}$ wavelength laser [20, 59]. In the limit of a relatively low amplitude laser pulse, $a_0 \ll a_{rad}$, the momentum of an electron moving in a circularly polarized electromagnetic wave in a plasma

scales with the laser pulse amplitude as $p = m_e c a_0$, while in the limit $a_0 \gg a_{rad}$, it scales as $p = m_e c (a_0 / \varepsilon_{rad})^{1/4}$.

Quantum effects become important, when the energy of the photon generated by Compton scattering is of the order of the electron energy, i.e. $\hbar\omega_m \approx \mathcal{E}_e$. An electron with energy $\mathcal{E}_e = \gamma m_e c^2$ rotates with frequency ω_0 in a circularly polarized wave propagating in a plasma and emits photons with frequency $\omega_m = \gamma^3 \omega_0$. We obtain that quantum effects come into play when $\gamma \geq \gamma_Q = \sqrt{m_e c^2 / \hbar \omega_0}$. For an electron interacting with one-micron laser light we find $\gamma_Q \approx 600$. From the previous analysis we obtain that the quantum limit on the electron gamma factor corresponds to

$$a_Q = \frac{2e^2 m_e c}{3\hbar^2 \omega_0}. \quad (15)$$

The energy flux reemitted by the electron is equal to $e(E \cdot v) = \varepsilon_{rad} \omega_0 \gamma^2 p_\perp^2 / m_e$. The total scattering cross section defined as the ratio of the reemitted energy to the Poynting vector $P = cE_0^2/4\pi$, is given by

$$\sigma = \sigma_T \frac{\gamma^2}{1 + \varepsilon_{rad}^2 \gamma^6}, \quad (16)$$

where the Thomson scattering cross section is $\sigma_T = 8\pi r_e^2/3 = 6.65 \times 10^{-25} \text{ cm}^2$. We see that, as the wave amplitude increases in the range $1 \ll a_0 \ll a_{rad}$, the scattering cross section increases according to the law $\sigma = \sigma_T(1 + a_0^2)$ and reaches its maximum $\sigma = \sigma_T a_{rad}^2$ at $a_0 \approx a_{rad}$; for $a_0 \gg a_{rad}$, it decreases according to the law $\sigma = \sigma_T a_{rad}^3 / a_0$. In Fig. 2 we show the scattering cross section dependence on the EMW amplitude and wavelength.

In the radiation-dominated regime of the EMW interaction with charged particles, i.e. at $a_0 > a_{rad}$, the emitted gamma quanta can produce secondary electron-positron pairs, which in turn emit gamma ray photons, producing an avalanche of γ rays and electron-positron pairs [60].

D. Probing Nonlinear Vacuum

When the amplitude of the electromagnetic wave approaches the critical electric field of quantum electrodynamics (also called the “Schwinger field”), vacuum becomes polarized and electron-positron pairs are created in vacuum [39, 61]. On a distance equal to the Compton length, $\lambda_C = \hbar/m_e c$, the work of the critical field on an electron is equal to the electron rest mass energy, $m_e c^2$, i.e. $eE_{QED}\lambda_C = m_e c^2$. The dimensionless parameter

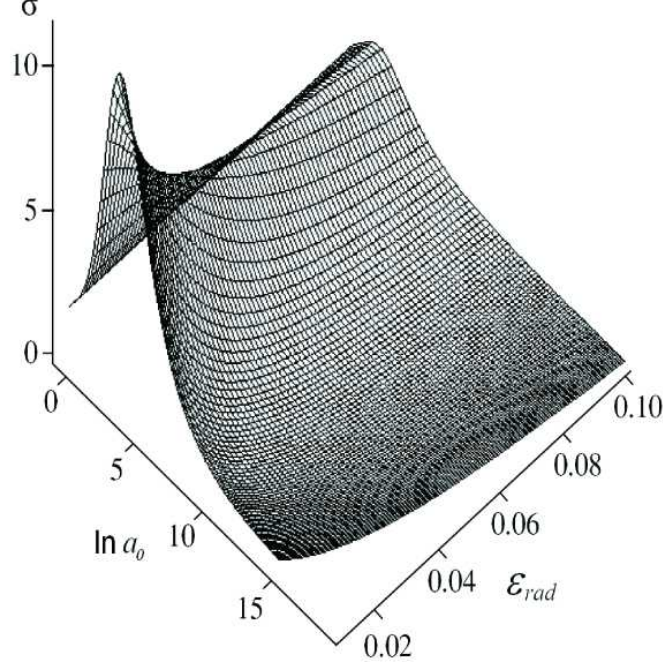


FIG. 2: Scattering cross section dependence on the EMW amplitude and wavelength.

$$\frac{E}{E_{QED}} = \frac{e\hbar E}{m_e^2 c^3} \quad (17)$$

becomes equal to unity for an electromagnetic wave intensity of the order of

$$I = \frac{c}{r_e \lambda_C^2} \frac{m_e c^2}{4\pi} \approx 4.7 \times 10^{29} \frac{W}{cm^2}. \quad (18)$$

For such ultrahigh intensities the effects of nonlinear quantum electrodynamics play a key role: an electromagnetic wave excites virtual electron-positron pairs. An observable manifestation of this process could be detection of light birefringence during the propagation of an electromagnetic wave in a strong electric or magnetic field in vacuum. The cross section for the photon-photon interaction in the limit $\hbar\omega \ll m_e c^2$ is given by

$$\sigma_{\gamma\gamma \rightarrow \gamma\gamma} = \frac{973}{10125} \frac{\alpha^2}{\pi^2} r_e^2 \left(\frac{\hbar\omega}{m_e c^2} \right)^6, \quad (19)$$

where $\hbar\omega$ is the photon energy (see [39]). This cross section reaches its maximum, $\sigma_{\max} \approx 10^{-20} cm^2$, for $\hbar\omega \approx m_e c^2$, i.e. for the interactions of photons in the gamma range. Also attention is focused on the process of electron-positron pair creation in vacuum by an electromagnetic wave. For an electric field small compared to E_{QED} , this process is sub-barrier, similarly to the tunnel ionization of atom discussed above [see Eq. (4)]. The

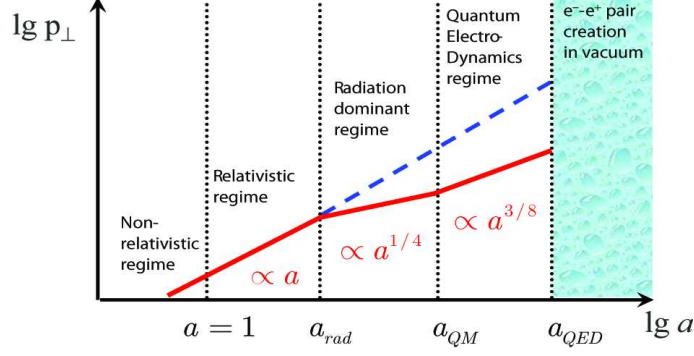


FIG. 3: Various regimes of relativistically strong EMW interaction with plasmas.

probability of electron-positron pair creation per unit volume and per unit time is exponentially small and is given by

$$w = \left(\frac{\alpha c}{\pi^2 \lambda_C^4} \right) \left(\frac{E}{E_{QED}} \right)^2 \exp \left(-\pi \frac{E_{QED}}{E} \right). \quad (20)$$

Here $\lambda_C = \hbar/m_e c$ is the Compton length and $\alpha = e^2/\hbar c = 1/137$ is the fine structure constant.

We may formally estimate the number of electron-positron pairs produced by a 10 fs long laser pulse in a volume $V = \lambda^3 = 10^{-12} \text{cm}^3$ as $N_{\pm} = wV\tau_p$. It is easy to show that N_{\pm} is equal to one pair for a laser intensity equal to $I = 10^{26} \text{W/cm}^2$ (a more detailed description of this process can be found in [65] and in Refs. [39, 62, 63]). Obviously, this latter number is overestimated because the minimum needed energy is by many orders of magnitude larger than the total energy of the laser pulse. At intensities of the order $I = 10^{30} \text{W/cm}^2$ Eq. (20) is not applicable and a depletion of the laser pulse must be taken into account. The electromagnetic pulse depletion due to its energy conversion into electron-positron pairs has been studied in Ref. [64].

The nonlinear dependence of the vacuum susceptibilities on the electromagnetic-field amplitude results in the finite value of the Kerr constant of vacuum. It can be found to be

$$K_K = \frac{7\alpha}{90\pi} \frac{\lambda_C^3}{m_e c \lambda_0} \quad (21)$$

The Kerr constant in vacuum for $\lambda_0 = 1 \mu\text{m}$ is of the order of $10^{27} \text{cm}^2/\text{erg}$, which is a factor 10^{20} smaller than for water. As shown in Ref. [32], in a QED nonlinear vacuum two counter-propagating electromagnetic waves mutually focus each other. A nonlinear modification of the refraction index in vacuum within the framework of the Heisenberg-Euler approximation

is characterized by the critical value of the electromagnetic wave power

$$\mathcal{P}_{QED} = 45\pi^2 \frac{cE_{QED}^2 \lambda_0^2}{4\pi\alpha}. \quad (22)$$

When the electromagnetic wave power exceeds this value, the cross modulation nonlinear effects affect the wave propagation. We see that the critical power, \mathcal{P}_{cr} , depends only on the laser pulse wavelength, λ_0 , and on fundamental constants. It is easy to show that for $\lambda_0 = 1\mu\text{m}$ the critical power $\mathcal{P}_{cr} = cE^2 w^2/4$, where w is the laser beam waist. For the mutual self-focusing $\mathcal{P}_{cr} = 2.5 \times 10^{24}\text{W}$ can be found to be for $\lambda_0 = 1\mu\text{m}$.

Nonlinear modifications of the vacuum refraction index lead to the vacuum birefringence [32], to the four-wave interaction [33], to the high order harmonic generation [34], and to the laser-photon splitting and merging [35] (see also review articles [13], [36, 37]). According to Ref. [31] the Unruh radiation intensity of the electron moving in the field of a strong electromagnetic wave becomes comparable with the nonlinear Thomson scattering intensity under the condition $4\pi a_0 \hbar \omega_0 / m_e c^2 \approx 1$. The multi-photon Compton scattering during the collision of counter-propagating laser beams and ultrarelativistic electron bunches leading to the gamma quanta generation

$$e^- + n\hbar\omega_0 \rightarrow \hbar\omega_\gamma, \quad (23)$$

with their subsequent interaction with the laser light accompanied by the electron -positron pair creation in vacuum via the Breit-Wheeler process

$$\hbar\omega_\gamma + n\hbar\omega_0 \rightarrow e^- + e^+ \quad (24)$$

has been investigated in Ref. [66]. In Ref. [67] the cross section of the Breit-Wheeler process on the laser pulse intensity has been investigated.

Various regimes of the relativistically strong EMW interaction with plasmas are illustrated in Fig. 3.

E. EMW Parameters under Space Plasma Conditions

In one of the first works on the charged particle acceleration by strong electromagnetic waves in astrophysical plasmas, pulsars [68] have been considered as sources of ultraintense radiation [70]. Pulsars are considered to be oblique rotators with non-parallel rotation and

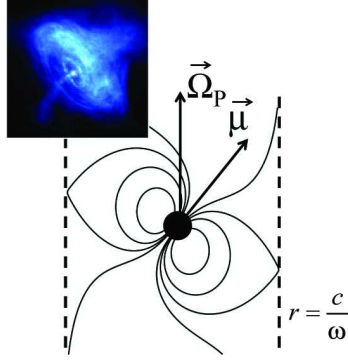


FIG. 4: Pulsar magnetosphere. The inset: The Crab pulsar [71].

magnetic dipole axes, as illustrated in Fig. 3. The power of magneto-dipole radiation is given by the expression

$$W = \frac{2\mu^2 \sin^2 \chi \Omega_P^4}{3c^3}, \quad (25)$$

where μ is the magnetic momentum, χ is an angle between the rotational and magnetic dipole axes, and Ω_P is the pulsar rotation frequency. Even for parallel magnetic and angular moments, i.e. for $\chi = 0$, the expression $W = (2/3)\mu^2\Omega_P^4/c^3$ gives the pulsar electromagnetic energy losses, as it follows from the theoretical model of the pulsar magnetosphere [69]. The magnetic moment is related to the pulsar magnetic field and radius as $\mu \approx Br_P^3$. For typical values of $r_P = 10^6$ cm and $B = 10^{12}$ G we obtain $\mu = 10^{30}$ G cm³. The electromagnetic wave intensity at the distance r is equal to $I = W/4\pi r^2$. At the wave zone boundary, $r = c/\Omega_P$, the dimensionless amplitude of the electric field is

$$a_P = \frac{e\mu\Omega_P^2}{m_e c^4}. \quad (26)$$

For the Crab pulsar with the rotation frequency $\Omega_P = 200$ s⁻¹ we find $a_P = 2 \times 10^{10}$.

According to Ref. [20, 59] in the limit of high radiation intensity the effects of the radiation damping should be incorporated into the theory of the electromagnetic wave interaction with plasmas. A dimensionless parameter,

$$\varepsilon_{rad} = \frac{2e^2\Omega_P}{3m_e c^3}, \quad (27)$$

gives a value of the wave amplitude, $a_{rad} = \varepsilon_{rad}^{-1/3}$, above which the radiation damping cannot be neglected. For $\Omega_P = 200$ s⁻¹ this yields $a_{rad} = 10^7$, which is substantially less than above found value of $a_P = 2 \times 10^{10}$.

In the case of laser - plasma interaction for a typical laser wavelength of $1\mu\text{m}$ the dimensionless amplitude a_{rad} corresponds to an intensity of the order of $10^{23}\text{W}/\text{cm}^2$ which can be achieved by tight focusing of the PW power laser beams onto the one-lambda size focus spot. We see that the laser plasmas can be used for modeling the radiation damping effects, which are important for relativistic astrophysics.

III. ACCELERATION OF CHARGED PARTICLES IN THE EMW INTERACTION WITH PLASMAS

General requirements for the laser accelerator parameters are principally the same as for standard accelerators of charged particles [73], i. e. they should have a reasonable acceleration scale length, a high enough efficiency and the required maximal energy, a high quality, emittance and luminosity of charged particle beams. In the 1940-s Enrico Fermi paid attention to the high energy limit of $\approx 1\text{PeV} = 10^{15}\text{eV}$ for accelerated particles, which could be reached under terrestrial conditions, when the accelerator size is limited by the equator circumference. These limitations resulted in the 1950-ties in the proposal to use collective electric fields excited in a plasma (collective methods of acceleration) in order to accelerate charged particles [24].

A. Electron Accelerator

Wakefield acceleration has been proposed in Ref. [18] for the generation of ultra high energy cosmic rays. Below we describe the wake field acceleration mechanism using as an example the LWFA scheme.

Under the condition of minimum laser energy the one stage LWFA accelerator scaling is described as it follows [16]. The electric field in a plasma has the form of a wave propagating with a phase velocity, $v_{ph,W}$. A gamma factor corresponding to the wave phase velocity is given by the expression $\gamma_{ph,W} = (1 - v_{ph,W}^2/c^2)^{-1/2}$. A condition of the wake wave synchronization with the driver laser pulse yields $v_{ph,W} = v_{g,las}$, where $v_{g,las} \approx c(1 - \omega_{pe}^2/2\omega_0^2)$ is the laser pulse group velocity. The wavelength of the weakly nonlinear wake wave is $\lambda_p = \lambda_0\gamma_{ph,W}$. Assuming the electrostatic potential in the wake is equal to $m_e c^2/e$, we obtain for the fast electron gamma factor $\gamma_e = 2\gamma_{ph,W}^2$. The acceleration length is given

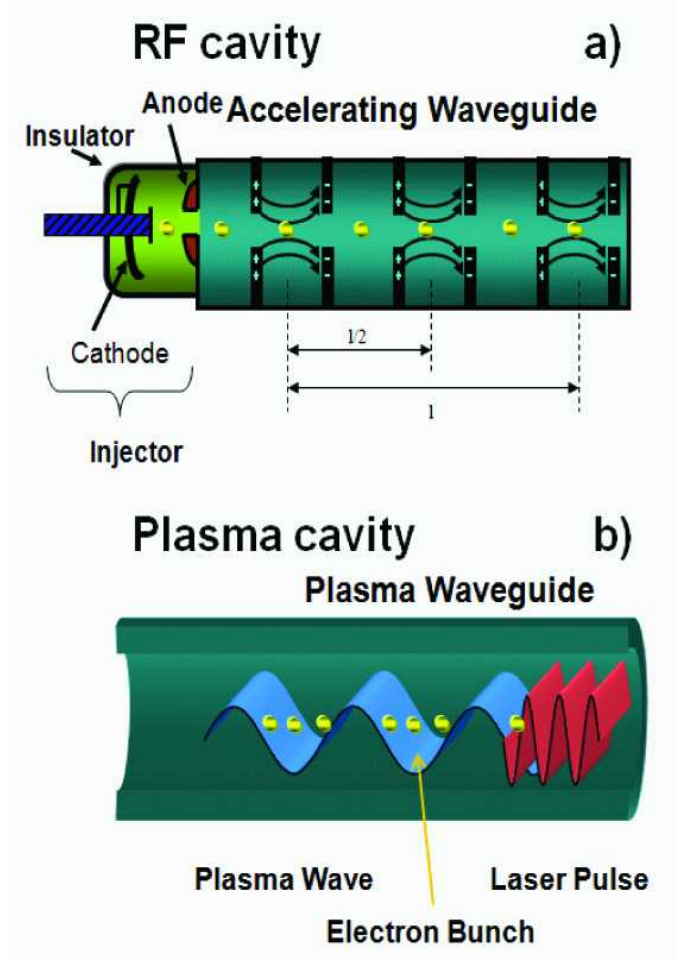


FIG. 5: Schematic view of the standard linear accelerator of charged particles, a) and the LWFA, b).

by $l_{acc} = \lambda_p \gamma_{ph,W}^2$, i.e. $l_{acc} = \lambda_0 \gamma_{ph,W}^3$. This gives a relationship between the acceleration length and the fast electron energy: $l_{acc} = \lambda_0 \gamma_e^{3/2}$. For $\lambda_0 = 1 \mu\text{m}$ and $\gamma_e = 10^6$ we obtain $l_{acc} \approx 1\text{km}$ [75].

In the opposite limit, when the laser transverse width $r_{las} \leq \lambda_p$, we need to take into account the formation of an electron density cavity moving with the group velocity of the laser pulse (see Fig.6, where the wake wave left behind the ultra short laser pulse in the underdense plasma is shown). The cavity's transverse size is determined by the laser pulse width and its length is of the order of the Langmuir wave wavelength. In this limit, the wavelength depends on the amplitude of the Langmuir wave, which in turn depends on the laser pulse intensity. For a given laser pulse width the electrostatic potential in the cavity is of the order of $\phi \approx \pi n_0 e r_{las}^2$, and the group velocity of a narrow laser pulse is determined

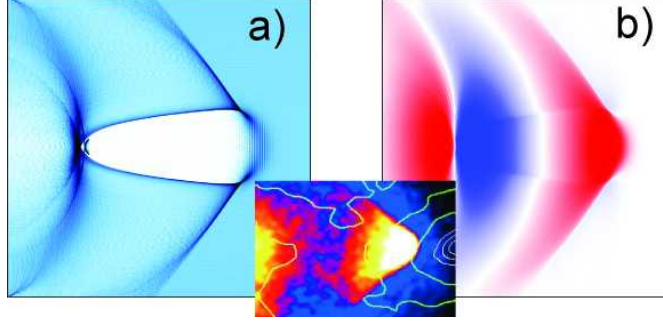


FIG. 6: 2D PIC simulations show that the electrons pushed away by the ponderomotive pressure of the laser pulse form the "bow wave" [49]. The electron density distribution (a) clearly shows the 'swallow-tail' formation during the wake wave breaking in the first period of the wave behind the laser pulse. The wakefield (the x-component of the electric field) is excited by the laser pulse in an underdense plasma (b). Inset: The bow wave formed by colliding galaxies in the Bullet Cluster [72].

by its width, i.e. $\gamma_{ph,W} \approx r_{las}/\lambda_0$. As a result we find the electron energy scaling [49]:

$$\gamma_e = \frac{r_{las}^4}{\lambda_0^2 \lambda_p^2}. \quad (28)$$

It does not depend on the laser pulse amplitude provided $a_0 > e\phi/m_e c^2$. The laser energy depletion length in this limit is given by

$$l_{dep} = a_0 l_{las} \left(\frac{\lambda_p}{\lambda_0} \right)^2, \quad (29)$$

i. e. it is by a factor a_0 greater than in the 1D case.

Considering the laser electron accelerator for the applications in the high energy physics, we find that its parameters should satisfy several conditions in addition to the requirement on the maximum particle energy. Parameters of fundamental importance such as the luminosity characterize the number of reactions produced by the particles in colliding beams of a collider. The luminosity is given by the expression

$$\mathcal{L} = f \frac{N_1 N_2}{4\pi \sigma_y \sigma_z}, \quad (30)$$

where N_1 and N_2 are the numbers of particles in each of the beams, σ_y and σ_z are the transverse size of the beam in the y and z directions, and f is the frequency of the beam collisions. A product of the luminosity and the reaction cross section gives the reaction

rate. We see that the luminosity can be increased by increasing the particle number in a bunch, N_j , and/or by increasing the repetition rate, f , or by decreasing the transverse size of the bunch, σ_i , by focusing the particle beam into the minimum size focal spot. The focal spot size depends on the beam emittance, which is defined as the surface occupied by the bunch in the phase plane $((y, p_y)$ or (z, p_z)). A calculation under the assumption of a round transverse shape of the beam ($\sigma_y = \sigma_z = r$) results in the expression given by the integral

$$\varepsilon_{\perp} = \frac{1}{\pi} \int dr dr', \quad (31)$$

where r is the transverse size of the bunch and $r' = dr/dx = dr/cdt$ [73].

The transverse dynamics of the electron in the field of the wake wave is described by the equation (see for example Ref. [76])

$$\frac{d}{dt} \left(\gamma_{\parallel} \frac{dr}{dt} \right) + \omega_{pe}^2 r = 0, \quad (32)$$

where the electron gamma factor depends on time as $\gamma_{\parallel}(t) = \gamma_e(1 - t^2/t_{acc}^2)$ with $\gamma_e = \gamma_{ph,W}^2$ and $\gamma_{ph,W} = \omega_0/\omega_{pe}$. In the limit $\gamma_{\parallel} \gg 1$ the electron transverse oscillations are described by the dependence of the radial displacement on time:

$$r(t) = r_{inj} \left(\frac{\gamma_{inj}}{\gamma_{\parallel}(t)} \right)^{1/4} \cos \left[\int_{t_{inj}}^t \omega_b(t') dt' \right], \quad (33)$$

where $\omega_b(t) = \omega_{pe}\gamma_{\parallel}(t)^2$ is the betatron oscillation frequency and r_{inj} and $\gamma_{inj} \approx \gamma_{ph,W}$ are the radial coordinate and the electron energy at the injection time, t_{inj} normalized on $m_e c^2$. Calculating the transverse emittance, we find $\varepsilon_{\perp} = \pi \kappa^2 (\omega_{pe}/\omega_0)^3$ mm mrad, with $\kappa = r_{inj}/\lambda_p$. The normalized emittance, $\varepsilon_N = \varepsilon_{\perp} \gamma_e$, is equal to $\varepsilon_N = \pi \kappa^2 (\omega_{pe}/\omega_0)$ mm mrad.

The electron motion in the electric field of the wake plasma wave is characterized by the structure of the phase plane $(p_x, X = x - v_{ph}t)$. A calculation of the energy spectrum of fast electrons is done in Refs. [76, 77]). It uses the property of electrons injected at the breaking point to move along the separatrix. The electrons, whose trajectories lie on the separatrix, where they are uniformly distributed, near the top of the separatrix have an electron momentum dependence on the coordinate

$$p_x = p_m(1 - X^2 \omega_{pe}^2 / c^2 a_0) = p_m(1 - t^2/t_{acc}^2). \quad (34)$$

The distribution function of the electrons at the target has the form

$$f(t, \mathcal{E}) = (n_b \omega_{pe} / \sqrt{2} c a_0) \delta(\mathcal{E} - \mathcal{E}_m(1 - t^2/t_{acc}^2)). \quad (35)$$

Here $\delta(z)$ is the Dirac delta function and we have assumed that the electrons are ultrarelativistic with $\mathcal{E} = p_x c$ and $\mathcal{E}_m = p_m c$. In order to find the energy spectrum of the electrons on the target, we must integrate the function on time in the limits between $-t_{acc}$ and t_{acc} . We obtain

$$\frac{d\mathcal{N}(\mathcal{E})}{d\mathcal{E}} = \frac{n_b \omega_{pe}}{\sqrt{2} c a_0} \int_{-t_{acc}}^{t_{acc}} \delta\left(\mathcal{E} - \mathcal{E}_m \left(1 - \frac{t^2}{t_{acc}^2}\right)\right) dt = \frac{n_b \omega_{pe}}{2\sqrt{2} c a_0 \sqrt{\mathcal{E}_m(\mathcal{E}_m - \mathcal{E})}}, \quad (36)$$

i.e. the particle spectrum has a typical form $\propto 1/\sqrt{\mathcal{E}_m - \mathcal{E}}$ near maximum energy.

Using the above given relationships and estimating a maximum number of particles in a bunch as $N \approx \kappa^2 n_e \lambda_p^3$, we obtain the luminosity to be equal to

$$\mathcal{L} = 10^{34} \left(\frac{f}{10 \text{ KHz}}\right) \left(\frac{\kappa}{0.1} \frac{\lambda_0}{r_{inj}}\right)^2 \left(\frac{\gamma_e}{10^6}\right)^{3/2} \frac{1}{\text{cm}^2 \text{s}}. \quad (37)$$

Here we assume a round transverse shape of the bunch with $r \approx r_{inj}(\gamma_{inj}/\gamma_e)^{1/4}$. Utilization of flat bunches with $\sigma_y \gg \sigma_z$ allows and to achieve larger luminosity [78]. In addition, in the case of flat beams the space charge effects and beamsstrahlung can be weakened. We notice that the radiation damping effects on the LWFA operation have been considered in Ref. [79].

B. Ion Accelerator

The mechanism of laser acceleration of ions (protons and other ions) is determined by the electric field set up by the space charge separation of hot or energetic electrons and the ions. The exact mechanisms entering into the energy transfer from the fast electron to the ion energy depends on the specific conditions of the laser-target interaction (see review articles [13] and [80]). The proton generation is a direct consequence of the electron acceleration.

The typical energy spectrum of laser accelerated particles observed both in experiments and in computer simulations can be approximated by a quasi-thermal distribution with a cut-off at a maximum energy. On the other hand, the applications require high quality proton beams, i.e. beams with sufficiently small energy spread $\Delta\mathcal{E}_i/\mathcal{E}_i \ll 1_i$. For example, for hadron therapy it is highly desirable to have a proton beam with $\Delta\mathcal{E}_i/\mathcal{E}_i \leq 2\%$ in order to provide the conditions for a high irradiation dose being delivered to the tumor, while sparing neighboring tissues. In Ref. [81] it was shown that such a required beam of laser

accelerated ions can be obtained using a double layer target. Extensive computer simulations of this target were performed in Ref. [82] and the results of experimental studies of this ion acceleration mechanism are presented in Ref. [83].

1. Ion acceleration during plasma expansion into vacuum

Ion acceleration during the collisionless plasma expansion into vacuum appears to be one of the most obvious mechanisms of the ion acceleration [84]. In particular, it has been considered as one of the possible acceleration mechanisms in space plasmas [14]. When the electrons that have been heated and tend to expand overtake the ions in a relatively small volume, the electric neutrality of the plasma breaks and the generated electric field induces the ion motion. Although a velocity of the bulk ion and electron motion is of the order of the ion acoustic speed, $v_s = \sqrt{T_e/m_p}$, a small fraction at the plasma front gains energy efficiently. Here T_e is the electron temperature and m_p is the ion (proton) mass. Under the most favorable conditions the ions achieve a kinetic energy which corresponds to an ion velocity of the order of the electron thermal velocity, i.e. the maximum ion energy can be of the order of $m_p \mathcal{E}_e/m_e$. We notice here that for the electron distributions with the energy cut-off this conclusion requires careful analysis (see Refs. [85, 86])

In the limit when the electron energy is relativistic, in order to analyze the ion motion one should use the equations of relativistic hydrodynamics, $\nu_\alpha T_\mu^\nu = 0$ with T_μ^ν being the energy-momentum tensor,

$$\partial_\mu (n u^\mu) = 0, \quad (38)$$

$$\mathcal{W} u^\mu \partial_\mu u^\nu = -(\delta^{\mu\nu} - u^\mu u^\nu) \partial_\mu P. \quad (39)$$

Here u^μ is the four-dimensional velocity vector, P is the pressure, n is the density in the proper frame of reference, $\mathcal{W} = P + \varepsilon$ is the enthalpy with ε being the internal energy density.

The self-similar plasma motion depending on the variable $\chi = x/t$ is described by a system of ordinary differential equations

$$\frac{u\chi - 1}{(u - \chi)(1 - u^2)} u' - (\ln n)' = 0, \quad (40)$$

$$\mathcal{W} \frac{u - \chi}{1 - u^2} u' - (u\chi - 1)P' = 0, \quad (41)$$

with a prime denoting a differentiation with respect to χ and $u = v/c$. Here we use the relativistic equation of state of an ideal gas,

$$\mathcal{W} = c^2 \frac{K_3(m_e c^2/T_e)}{K_2(m_e c^2/T_e)}, \quad (42)$$

$$P = nT_e, \quad (43)$$

where $K_n(x)$ are the modified Bessel functions. In the case of $T_e = \text{constant}$ we find

$$u = \frac{c_s + c\eta}{c + c_s}, \quad (44)$$

$$n = n_0 \left(\frac{c_s - c\eta}{c + c_s} \right)^{c/c_s} \quad (45)$$

with c_s being the relativistic speed of sound,

$$c_s = \sqrt{\frac{T_e}{m_e} \frac{K_3(m_e c^2/T_e)}{K_2(m_e c^2/T_e)}}. \quad (46)$$

In the ultra-relativistic limit the energy spectrum of fast ions has a power-law form,

$$\frac{d\mathcal{N}_p(\mathcal{E}_i)}{d\mathcal{E}_i} \propto \mathcal{E}_i^{-2c^2/c_s^2}. \quad (47)$$

2. Radiation pressure dominated regime of the ion acceleration

A regime of ion acceleration that exhibits very favorable properties has been identified in Ref. [19]. Among the wide variety of ion acceleration mechanisms realized in the laser-plasma interaction, the radiation pressure dominated ion acceleration (RPDA) has the highest efficiency. In the RPDA ion accelerator the laser pulse radiation pressure pushes forward the irradiated region of a thin foil as a whole. In the relativistic limit, when the electrons and ions move together with the same velocity due to a smallness of the electron to ion mass ratio, the ion kinetic energy is by a factor m_i/m_e times higher than the electron energy. In this case the laser pulse interacts with an accelerated foil like with a relativistic co-propagating mirror. The electromagnetic radiation reflected back by the relativistic mirror has almost negligible energy compared to the energy in the incident laser pulse, i.e. the laser energy is almost completely transformed into the energy of fast ions. In Fig. 7 we show results of 3D PIC simulations of this ion acceleration regime. In the course of the interaction with a thin overdense plasma slab the multi-petawatt laser pulse forms a cocoon

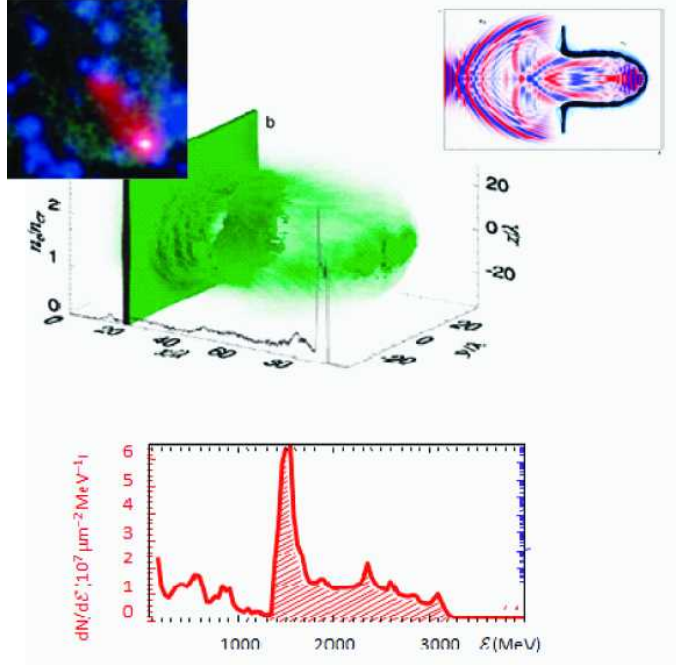


FIG. 7: Results of 3D PIC simulations of the PPDA ion acceleration regime. a) The electromagnetic pulse forms a cocoon confining the EMW energy. The right inset shows a cocoon seen in the plasma density and an EMW distribution obtained with the 2D PIC simulation. In the left inset we see a cocoon formed by the Black Widow pulsar (Pic. NASA). b) Quasi-monoenergetic ion spectrum.

confining the EMW energy, thus increasing the coupling of the electromagnetic wave with the target (see frame a) and the 2D inset). The ions accelerated beyond the GeV energy level have a quasi-monoenergetic spectrum (Fig. 7b). We notice that a combination of the RPDA mechanism with the use of double layer targets can substantially increase the ion acceleration efficiency as demonstrated in Ref. [26].

The equations of the irradiated foil motion can be cast into the form [87]:

$$\frac{dp_i}{dt} = \mathcal{P} d\sigma_i, \quad (48)$$

where p_i is a momentum of the foil element, $d\sigma_i$ is a vector normal to the foil, the index $i = 1, 2, 3$, and \mathcal{P} is the relativistically invariant pressure. In the frame of reference co-moving with the foil the radiation pressure is equal to $\mathcal{P} = E_M^2/2\pi$, with E_M being the EMW amplitude. In the laboratory frame of reference we have $E_0^2 = E_M^2 (\omega_0/\omega_M)^2$, where ω_0 and ω_M are the wave frequency in the laboratory and boosted frames. They are related

to each other as $\omega_M/\omega_0 = \sqrt{(1-\beta)/(1+\beta)}$. Introducing the Lagrange variables η and ξ , related to the Euler coordinates as $x = x(\eta, \xi, t)$, $y = y(\eta, \xi, t)$, $z = z(\eta, \xi, t)$, we find that the vector normal to the foil surface element is given by $d\sigma_i = \varepsilon_{ijk} dx_j dx_k$. Here dx_j are the vectors directed along the i -axes, ε_{ijk} is the fully antisymmetric unity tensor, and a summation over repeated indices is assumed. Using these relationships we can find the equations of foil motion

$$\frac{\partial p_i}{\partial t} = \frac{\mathcal{P}}{\nu_0} \varepsilon_{ijk} \frac{\partial x_j}{\partial \eta} \frac{\partial x_k}{\partial \xi}, \quad (49)$$

$$\frac{\partial x_i}{\partial t} = c \frac{p_i}{\sqrt{m_p^2 c^2 + p_k p_k}}. \quad (50)$$

Here $\nu_0 = n_0 l_0$ is the initial surface density, $p_i = (p_x, p_y, p_z)$ is the momentum, $x_i = (x, y, z)$ is the foil element coordinate and, the index, m_p is the ion mass. In the nonrelativistic limit for constant pressure \mathcal{P} , this system is reduced to the equations obtained in Ref. [88].

When a planar foil is irradiated by a normally incident EM pulse, the ions achieve the energy

$$\gamma_i = 1 + \frac{2w^2}{1 + 2w}, \quad (51)$$

where w is the normalized fluence,

$$w = \int_{-\infty}^{t-x/c} \frac{E_0^2(\psi)}{2\pi n_0 l m_i c} d\psi. \quad (52)$$

In the limit $w \gg 1$ the resulting ion energy is equal to the ratio of the laser pulse energy, \mathcal{E}_{las} , to the total number of accelerated ions, N_{tot} , i.e. $\gamma_i \approx \mathcal{E}_{las}/m_i c^2 N_{tot}$. As an example, we consider a solid density foil, $n_0 = 10^{24} \text{cm}^{-3}$, of $1 \mu\text{m}$ thickness irradiated by a laser pulse with a transverse size of $100 \mu\text{m}$. For the laser pulse energy of the order of 200 kJ we find that the accelerated ion energy is equal to 1 TeV with a total ion number of 10^{12} . The ion acceleration length in this case is approximately equal to $l_{acc} \approx 0.5 \text{ km}$.

In order to achieve high values of the ion bunch luminosity it is highly desirable to decrease the transverse bunch size. This can be achieved by modulating the density inside the foil, e.g. by a properly modulated laser pulse. The analysis of the linearized equations of the foil motion demonstrates the exponential growth of the modulations

$$x_i^{(1)}(\alpha, \beta, t) \propto \exp \left[\left(\frac{t}{\tau_{RT}} \right)^{1/3} - iq\eta - ir\xi \right], \quad (53)$$

where

$$\tau_{RT} = \omega_0^{-1} \frac{(2\pi)^{3/2} R_0^{1/2}}{6 (q^2 + r^2)^{3/2} \lambda_0^2}. \quad (54)$$

and [87]

$$R_0 = \frac{E_0^2}{2\pi n_0 l \omega_0^2}.$$

This opens a way for focusing the accelerated ions onto a narrow spot with lower limit given by the foil thickness. Using these results we can estimate the RPDA accelerated ion bunch luminosity as

$$\mathcal{L} = 10^{35} \left(\frac{f}{10 \text{ KHz}} \right) \left(\frac{N_{tot}}{10^{12}} \right)^2 \left(\frac{10^{-4} \text{ cm}}{\sigma_{\perp}} \right)^2 \frac{1}{\text{cm}^2 \text{ s}}. \quad (55)$$

A first indication of the RPDA - regime has been obtained in the experiments [89], when a thin foil target has been irradiated by a laser pulse with an intensity approaching 10^{20} W/cm^2 .

IV. MINI-BLACK-HOLES ON EARTH

We may see that when LWFA and RPDA accelerators will reach 100 GeV and TeV particle energies, which corresponds to the energy range of interest for high energy physics, laser accelerators may be considered as a source of ultrarelativistic particle beams with parameters comparable to those, which are produced by standard accelerators.

As an example for the problems in the field of high energy physics and astrophysics which may be explored with laser accelerators of charged particles, we note the mini-black-hole detection. In the general relativity theory black holes play a fundamental role. The Einstein equation [53, 90],

$$R_{\mu\nu} - \frac{1}{2} g_{\mu\nu} R = -\frac{8\pi}{m_p^2} T_{\mu\nu}, \quad (56)$$

where $m_p^2 = 1/G$ is the square of the Planck mass, and $T_{\mu\nu}$ is the energy-momentum tensor (the units $\hbar = c = 1$ are used), has a Schwarzschild solution for the interval:

$$ds^2 = g_{\mu\nu} dx^\mu dx^\nu = -\eta(r) dt^2 + dr^2 / \eta(r) + r^2 d\Omega^2 \quad (57)$$

with

$$\eta(r) = 1 - (2/m_p^2) M/r. \quad (58)$$

Here M and Ω are the object mass and the surface element in the 3D space. The metric given by this interval has a singularity at r equal to the Schwarzschild radius, $R_{BH} = 2M/m_p^2$. For an object with a mass of the order of the solar mass the black hole radius is equal to 2 km.

As it was noted above, a black hole with the size of about the Planckian length, 10^{-33} cm, has the mass $m_p = 10^{-5}$ g, which corresponds to an energy approximately equal to 10^{19} GeV.

The situation may change, if our world's dimension is higher than 3. In accordance with modern quantum field theory [91], our world may have higher dimensions $(d + 3)$. The additional dimensions are compactified in a sufficiently small scale, R_{comp} . Gravitational interaction is present in the whole space due to its universal character. At the small scale for $r \ll R_{comp}$, the gravitational potential of the field produced by an object with mass M behaves as $\phi(r) = M_f^{d+2} M / r^{(1+d)}$. A constant M_f characterizes the gravitational interaction in the small scale limit. In the limit of large scale compared with R_{comp} , i.e. for $r \gg R_{comp}$ we have the expression $\phi(r) = M / m_p^2 r = M / r R_{comp}^d M_f^{d+2}$. It yields a relationship between m_p , R_{comp} , and M_f being $m_p^2 = M_f^{d+2} R_{comp}$. The solution of the Einstein equation in space with $d+3$ dimension gives for the interval the formula

$$ds^2 = -\eta(r)dt^2 + dr^2/\eta(r) + r^2 d\Omega_{d+3}^2, \quad (59)$$

where Ω_{d+3} is the surface element and the metric element is equal to

$$\eta(r) = 1 - (R_{BH}/r)^{d+1}. \quad (60)$$

This results in the expression for the black hole radius

$$R_{BH}^{d+1} = (2/(d+1)) M_f^{-(d+1)} M / M_f. \quad (61)$$

For the constant M_f of the order of 1 TeV the black hole radius is equal to $R_{BH} \approx 10^{-4}$ fm (here 1 fm = 10^{-13} cm). A probability of a black hole creation is proportional to the cross section of this process [10]

$$\sigma_{BH} = \pi R_{BH}^2. \quad (62)$$

In the collision of 7 TeV proton bunches with a luminosity of the order of the LHC luminosity, $\mathcal{L} = 10^{34} \text{ cm}^{-2} \text{ s}^{-1}$, it is expected that approximately 10^9 mini-black-holes may be detected per year. The created mini-black-holes are to be detected by their emission of electromagnetic radiation and of elementary particles according to the Hawking mechanism. At the end of its evolution the black hole is thought to be strings.

The TeV range laser accelerator of charged particles can generate 10^6 mini-black-hole per year, when its repetition rate is 1 Hz.

V. FLYING MIRROR CONCEPT OF THE ELECTROMAGNETIC WAVE INTENSIFICATION

An electromagnetic wave reflected off a moving mirror undergoes frequency multiplication and corresponding increase in the electric field magnitude. The multiplication factor $(1 + \beta_M)/(1 - \beta_M)$ is approximately proportional to the square of the Lorentz factor of the mirror, $\gamma_M = 1/\sqrt{1 - \beta_M^2}$, making this effect an attractive basis for a source of powerful high-frequency radiation. Several ways have been suggested to extremely high intensity (see articles, Refs. [29, 92, 93], [13, 110] and literature quoted in). A specular reflection by a sufficiently dense relativistic electron cloud as suggested in Refs. [94]. The reflection at the moving ionization fronts was studied in Refs. [95].

Here we consider the “flying mirror” concept[29]. It uses a fact that at optimal conditions, the dense shells formed in the electron density in a strongly nonlinear plasma wake, generated by a short laser pulse, reflect a portion of a counter-propagating laser pulse. In the wake wave generated by the ultrashort laser pulse electron density modulations take the form of a paraboloid moving with the phase velocity close to the speed of light in vacuum [98]. At the wave breaking threshold the electron density in the nonlinear wake wave tends towards infinity. The formation of peaked electron density maxima breaks the geometric optics approximation and provides conditions for the reflection of a substantially high number of photons of the counterpropagating laser pulse. As a result of the electromagnetic wave reflection from such a “relativistic flying mirror”, the reflected pulse is compressed in the longitudinal direction, which is a consequence of frequency upshifting. The paraboloidal form of the mirrors leads to a reflected wave focusing into the spot with the size determined by the shortened wavelength of the reflected radiation (see Fig. 8). This mechanism allows to generate extremely short, femto-, atto-, zepto-second duration pulses of coherent electromagnetic radiation with extremely high intensity, which pave the way for studying such nonlinear quantum electrodynamics effects as the electron-positron pair creation and nonlinear refraction in vacuum.

The key parameter in the problem of Flying Relativistic Mirror (FRM) is the wake wave gamma factor, $\gamma_{ph,W}$. According to the special theory of relativity [96], the frequency of the electromagnetic wave reflected from FRM increases by a factor approximately equal to $4\gamma_{ph,W}^2$. A number of back reflected photons is proportional to $\gamma_{ph,W}^{-3}$ (for details see Ref.

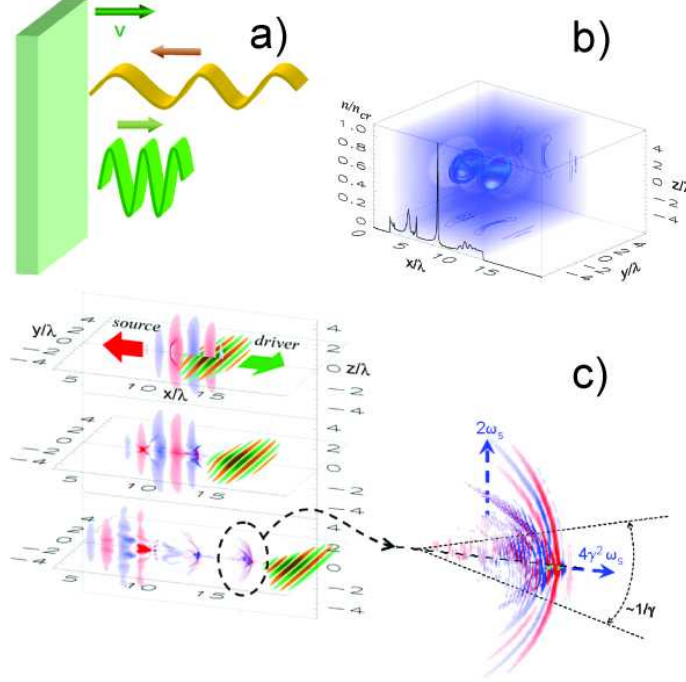


FIG. 8: Flying Mirror Concept. a) The reflection of EMW at the relativistic mirror results in a frequency upshifting and compression of the wave. b) Paraboloidal modulations of the electron density in the plasma wake wave. c) The electric field pattern of the laser pulse driver and of the reflected EMW. Inset: The reflected electromagnetic pulse frequency is upshifted, it is focused and its intensity increases.

[97]), which results in the reflected light intensification [29]

$$I_r/I_0 \approx \gamma_{ph,W}^3 (S/\lambda_0)^2, \quad (63)$$

where S is the transverse size of the laser pulse incident on the FRM. The reflected pulse power increases as $\mathcal{P}_r = \mathcal{P}_0 \gamma_{ph,W}$.

Using the expression for the reflected pulse intensity (63), we obtain that the interaction of two laser pulses with energies 10 kJ and 30 J, respectively, counterpropagating in a plasma with a density $\approx 10^{18} \text{cm}^{-3}$ can result in a light intensification of up to $\approx 10^{28} \text{W cm}^{-2}$. This corresponds to the generation of an electric field with a value close to the nonlinear quantum electrodynamics (QED) limit, $E_{QED} = m_e^2 c^3 / e \hbar$, when electron-positron pairs can be created in vacuum. This QED electric field is also called the "Schwinger field".

Experiments utilizing the electromagnetic pulse intensified with the FRM technique may allow studying regimes of super-Schwinger fields, when $E > E_{QED}$. This may be possible

because the light reflected by the paraboloidal FRM is focused into a focus spot moving with a relativistic velocity and is well collimated within an angle $\approx 1/\gamma_{ph,W}$ [29]. The wave localization within the narrow angle corresponds to the fact that the wave properties are close to the plane wave properties to the extent of the smallness of the parameter $1/\gamma_{ph,W}$. In this case the second Poincare invariant of the electromagnetic field, $B^2 - E^2$, has a value of the order of $E^2/\gamma_{ph,W}^2$. Therefore the electric field amplitude in the reflected electromagnetic wave can exceed the Schwinger limit by $\gamma_{ph,W}$ times. We note that a tightly focused electromagnetic wave cannot have an amplitude above E_{QED} , due to the electron-positron pair creation [65] when $E \rightarrow E_{QED}$ leads to the depletion of the electromagnetic wave [64].

As it was shown above, the critical power for mutual focusing of two counterpropagating EMW is equal to $\mathcal{P}_{cr} = 2.5 \times 10^{24} \text{W}$, which is beyond the reach of existing and planned lasers. Fortunately, if we take into account that the radiation reflected by the FRM has a shortened wavelength $\lambda_r = \lambda_0/4\gamma_{ph,W}^2$ and that its power is increased by a factor $\gamma_{ph,W}$, we may find that for $\gamma_{ph,W} = 30$, i.e. for a plasma density $\approx 3 \times 10^{17} \text{cm}^{-3}$, nonlinear vacuum properties can be seen for laser light the incident on the FRM with a power of about 10 PW. This makes the FRM concept attractive for the purpose of studying nonlinear quantum electrodynamics effects.

Within the framework of the Flying Mirror concept, it has been demonstrated [29] that the wavelength of the laser pulse, which has been reflected and focused at the wake plasma wave, becomes shorter by a factor $4\gamma_{ph}^2$ and its power increases by a factor $2\gamma_{ph}$. From this it follows that nonlinear QED vacuum polarization effects are expected to be observable for 50 PW 1- μm lasers.

A demonstration of the Flying Mirror concept has been accomplished in the experiments of Ref. [99]. Two beams of terawatt laser radiation interacted with an underdense plasma slab. The first laser pulse excited the nonlinear wake wave in a plasma with parameters required for the wave breaking, which has been seen in the quasi-mono-energetic electron generation and in the stimulated Raman scattering. The second counter-crossing laser pulse has been partially reflected from the relativistic mirrors formed by the wake plasma wave. We detected the electromagnetic pulses with a duration of femtoseconds and wavelengths from 7 nm to 15 nm. These results demonstrate the feasibility of constructing sources of coherent X-ray radiation with the parameters that are tunable in a broad range.

VI. RECONNECTION OF MAGNETIC FIELD LINES & VORTEX PATTERNS

The term "magnetic field line reconnection" refers to a broad range of problems that are of interest for space and laboratory plasmas. The results of theoretical and experimental studies of magnetic reconnection have been reviewed in many papers and monographs [14, 102, 103]. As it concerns relativistic laser plasmas, earlier a conclusion was made in Ref. [104] about the important role of the generation of magnetic fields by fast electron currents and their reconnection in the relativistic laser-matter interaction regime. The experiments conducted in Refs. [105] revealed magnetic reconnection phenomena in laser plasmas, when two high power laser beams irradiated a thin foil target.

Processes of reconnection are accompanied by an ultra fast magnetic energy release, which is transformed into different forms, such as internal plasma energy, radiation and fast particles.

A. Dimensionless parameters describing the relative roles of nonlinear, dissipative and Hall effects

Inside current sheets, which are basic entities in the reconnection process, as well as in the vicinity of shock wave fronts, the effects of dissipation and of nonlinearity play a crucial role being comparable in magnitude. Together with the Hall effect, which leads to the appearance of small scale structures, these effects violate the freezing of magnetic field in plasma motion.

Magnetic field is frozen in a plasma in the limit of a large Lundquist number $S \rightarrow \infty$. It obeys the equation:

$$\partial_t \mathbf{B} = \mathbf{v} \times \mathbf{B}, \quad (64)$$

which corresponds to the conservation of magnetic field flux through a contour moving with the plasma. The dimensionless parameter S is equal to the ratio of two characteristic time scales: the magnetic diffusion time $\tau_\sigma = l^2/\nu_m$ and a typical time $\tau_A = l/v_A$ that it takes for an Alfvén wave to propagate along the distance l ; $S = \tau_\sigma/\tau_A$. Here the magnetic diffusivity is $\nu_m = c^2/4\pi\sigma$, where σ is the electric conductivity of the plasma, and $v_A = |\mathbf{B}|/\sqrt{4\pi\rho}$ is the Alfvén wave velocity.

In the vicinity of the zero point the scale of the field nonuniformity l equals to the distance

r from the zero point. The magnetic field and hence the Alfvén velocity are proportional to r : $|\mathbf{B}| = hr$, $v_A = hr/\sqrt{4\pi\rho} \equiv \Omega_A r$. Here h is a typical value of the gradient of the magnetic field.

The measure of the significance of nonlinear effects is given by the ratio $\delta B/hl$ between the magnitude of the magnetic field perturbation δB and the background magnetic field $B = hl$. This ratio depends on the distance from the null point, due to both the nonuniformity of the background magnetic field B and to the change of the MHD wave amplitude in the course of its propagation.

If the plasma is pinched by a the quasi-cylindrical electric current I with a radius of the order of r , the value of the magnetic field at its boundary is approximately $\delta B = 2I/cr$. The dimensionless ratio $\delta B/hl$ is equal to one for $r \approx r_m = \sqrt{I/hc}$. If the electric current has the form of a quasi-one-dimensional slab pinch, and if the pinching occurs in the direction of its small size, the characteristic value of the magnetic field perturbation is constant: $\delta B = B_{\parallel}$ and the ratio ε becomes of order unity at the distance $r_A = B_{\parallel}/h$. In the approximation of small amplitude perturbations, these two types of pinching correspond to the effects of the propagation of magnetoacoustic and of Alfvén waves, respectively. The magnetoacoustic waves focus towards the null line, while the energy of the Alfvén waves accumulate near the magnetic field separatrices. The values r_m and r_A determine the size of the region, where the magnetoacoustic wave and, respectively, the Alfvén one become nonlinear.

The dimensionless parameters

$$(r_m/r_{\sigma})^2 = I\Omega_A/c\nu_m \equiv L_m, \quad (65)$$

$$(r_A/r_{\sigma})^2 = B_{\parallel}^2\Omega_A/h^2\nu_m \equiv L_A \quad (66)$$

determine the relative role of the dissipation and of the nonlinearity effect in the course of the current sheet formation due to finite amplitude perturbations of the magnetoacoustic and of the Alfvén wave type, respectively.

Now we discuss the relationship between the dimensionless parameter L_m and the current sheet parameters obtained in the framework of the Sweet – Parker model [106, 107]. In this model it is supposed the current sheet has a width b and a thickness a with $b \gg a$. The plasma flows into the current sheet with a velocity $v_{\text{in}} \approx \nu_m/a$ and exits through its narrow edges with a velocity v_{out} , which is of the order of the Alfvén wave velocity, $v_A \approx \Omega_A b$. From mass conservation we obtain $v_{\text{in}}b = av_{\text{out}}$. From this it follows that the thickness of the

current sheet is equal to

$$a = \sqrt{\nu_m/\Omega_A}, \quad (67)$$

i.e. of order r_σ . Estimating the current sheet width as r_m , we find that the ratio of its width to its thickness is

$$b/a = \sqrt{I\Omega_A/hc\nu_m} \equiv \sqrt{L_m}. \quad (68)$$

Thus, the condition for the formation of a wide current sheet with $b \gg a$ is equivalent to the requirement $L_m \gg 1$. Similarly, current sheets are formed in the vicinities of the magnetic field separatrices when $L_A \gg 1$.

Considering the case when the Hall effect, i.e. the electron inertia, plays a dominant role in the reconnection process, we define the dimensionless parameter which measures the role of the Hall effect as $\tilde{\alpha} = \alpha h/\Omega_A l \equiv c/\omega_{pi} l$. When the length r_H , at which the Hall effect starts to be important, is larger than the current sheet thickness, $r_H/a = \alpha h/\sqrt{\nu_m\Omega_A} > 1$, the effects of dispersion lead to the formation of small scale structures. In the limit $r_H/b = \alpha h\sqrt{ch/I}/\Omega_A \gg 1$ the pattern of the plasma flow is completely determined by the Hall effect. Similar to the way used to define the parameters L_m and L_A , we define the dimensionless parameter

$$L_H = (b/r_H)^2 = E^2 c^2 \Omega_A / h^4 \alpha^2 \nu_m \equiv E^2 \omega_{pi}^2 / h^2 \nu_m \Omega_A. \quad (69)$$

When $L_H \gg 1$, nonlinear effects are much stronger than the Hall effect.

B. Current Sheet

In a simple 2D configuration the current sheet is formed in the magnetic field described by a complex function $B(x, y) = B_x - iB_y = h\zeta$ of a complex variable $\zeta = x + iy$. The magnetic field vanishes at the coordinate origin. The magnetic field lines lie on the surfaces of constant vector potential, $A(x, y) = \text{Re}\{h\zeta^2/2\}$. They are hyperbolas as we can see in Fig. 9 a). This is a typical behaviour of the magnetic field lines in the vicinity of null lines (they are the so called X-lines) in magnetic configurations. Under finite time perturbations the magnetic X-line evolves to the magnetic configurations of the form $B = h(\zeta - b)^{1/2}$, which describes the magnetic field created by thin current sheet between two points $\pm b$ [102]. The magnetic field lines lie on the constant surfaces of

$$A(x, y) = \frac{h}{2} \text{Re} \left\{ \zeta \sqrt{\zeta^2 - b^2} - \text{Log} \left[\zeta + \sqrt{\zeta^2 - b^2} \right] \right\}. \quad (70)$$

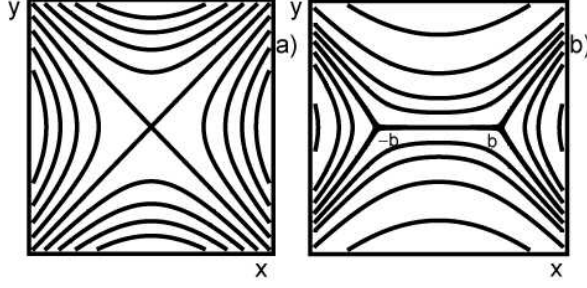


FIG. 9: Magnetic field pattern in the vicinity of the X-line (a). Current layer formed in the vicinity of the X-line (b).

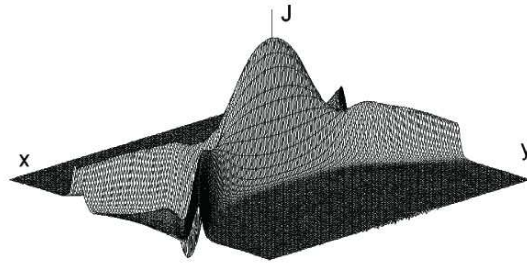


FIG. 10: Electric current density distribution inside the current sheet [108].

They are shown in Fig. 9 b. The width of the current layer b is determined by the total electric current I inside, and by the magnetic field gradient, h . It is equal to

$$b = \sqrt{4I/hc}. \quad (71)$$

In the strongly nonlinear stage of the magnetic field and plasma evolution a quite complex pattern in the MHD flow in the nonadiabatic region near the critical point can be formed, with shock waves and current sheets. In Fig. 10 we show the results of the dissipative magnetohydrodynamics simulations of the current sheet formation near the X-line.

C. Magnetic Reconnection in Collisionless Plasmas

When the Hall effect is dominant, i.e. the electron inertia determines the relationship between the electric field and the electric current density carried by the electron component, the magnetic field evolution is described by the equation (see [116, 117])

$$\partial_t(\mathbf{B} - \Delta\mathbf{B}) = \nabla \times [(\nabla \times \mathbf{B}) \times (\mathbf{B} - \Delta\mathbf{B})], \quad (72)$$

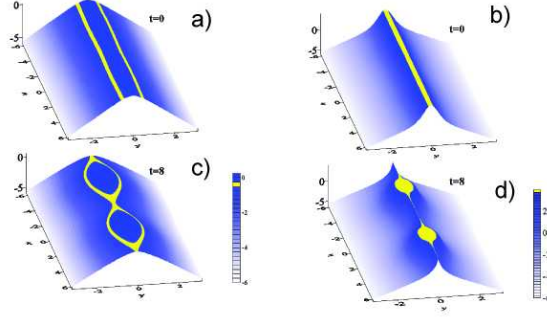


FIG. 11: Nonlinear stage of the development of the tearing mode instability in a current sheet: a) the magnetic field and b) the generalized vorticity distribution at $t=0$. The same functions at $t=8$ in c) and d).

which corresponds to the condition of generalized vorticity, $\Omega = \mathbf{B} - \Delta \mathbf{B}$, be frozen into the electron component motion with the velocity $\mathbf{v}_e = c \nabla \times \mathbf{B} / 4\pi n_0 e$. Here the space scale is chosen to be equal to the collisionless electron skin-depth, $d_e = c/\omega_{pe}$, and the time unit is $\omega_{Be}^{-1} = m_e c / e B$. The range of frequencies described by the EMHD equations is given by $\omega_{Bi} < \omega < \omega_{Be}$.

In the linear approximation Eq. (72) describes the propagation of whistler waves, for which the relationship between the wave frequency and the wave vector, is $\omega = |\mathbf{k}|(\mathbf{k} \cdot \mathbf{B}_0)/(1 + k^2)$. From this relationship it follows that in a weakly inhomogeneous magnetic field the critical points are the points and lines where $|\mathbf{B}_0| = 0$ or/and $(\mathbf{k} \cdot \mathbf{B}_0) = 0$.

The electron inertia effects make the reversed magnetic field configuration unstable against tearing modes [118?], which result in magnetic field line reconnection. The slab equilibrium configuration with a magnetic field given by $\mathbf{B}_0 = B_{0z} \mathbf{e}_z + B_{0x}(y/L) \mathbf{e}_y$, where $B_{0x}(y/L)$ is the function that gives the current sheet magnetic field, is unstable with respect to perturbations of the form $f(y) \exp(\gamma t + i k x)$ with $kL < 1$. For this configuration one has $(\mathbf{k} \cdot \mathbf{B}_0) = 0$ at the surface $y = 0$. The growth rate of the tearing mode instability is [117, 119, 120] $\gamma \approx (1 - kL)^2 \Delta'^2 / kL^2$.

In Fig. 11 the results of a numerical solution of Eq. (72) in a 2D geometry with magnetic field $\mathbf{B}(x, y, t) = (\nabla \times a) \times \mathbf{e}_\perp + b \mathbf{e}_\parallel$ are shown. The unperturbed configuration is chosen to be a current sheet, infinite in the x -direction, that separates two regions with opposite magnetic field. Both the line pattern of generalized vorticity, $\Omega = a - \Delta a$, and of the magnetic field show the formation of quasi-one-dimensional singular distributions in the

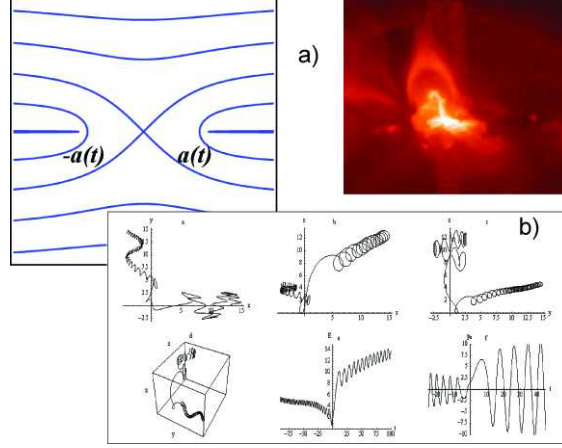


FIG. 12: a) The current sheet break up into two parts separated by the distance $2a(t)$. b) The projections of the trajectory of charged particle accelerating in the vicinity of the magnetic X-line. Inset: The solar flare (YOHKOH image).

electric current density and in the distribution of the generalized vorticity. The magnetic field topology changes, as is seen from Fig. 11.

D. Charged Particle Acceleration

A fully developed tearing mode results in a current sheet break up into parts separated by a distance $2a$, as it is illustrated in Fig. 12a (see. Ref. [102] and literature quoted therein). Under the magnetic field line tension the plasma is thrown out. The model magnetic field describing this configuration is given by the complex variable function $B(\zeta) = B_0\zeta/\sqrt{a^2 - \zeta^2}$. The magnetic field lines lie on the surfaces of constant vector potential,

$$A(x, y, t) = \text{Re} \left\{ B_0 \sqrt{a^2(t) - \zeta^2} \right\}. \quad (73)$$

Due to a dependence of the function a on time the electric field parallel to the z axis arises. It is given by

$$E(x, y, t) = -\frac{1}{c} \partial_t A = -\frac{1}{c} \frac{B_0 a(t) \dot{a}(t)}{\sqrt{a^2(t) - \zeta^2}}. \quad (74)$$

In the vicinity of the null line we have a quadrupole structure of the magnetic $B(\zeta) \approx B_0\zeta/a$ field and a locally homogeneous electric field, $E \approx \dot{a}B_0/c$.

The magnetic field reconnection, the study of which has been started by Dungey [121], on its initial stage had had as a main goal to explain the generation of suprathermal particles

during solar flares and substorms in the earth's magnetosphere. Despite the simplicity of the formulation of the problem, it is quite far from a complete solution. Even in the test particle approximation, which describes the particle motion in the given magnetic and electric fields, the solution of this problem meets serious difficulties [14, 101]. The reason of that is due to the fact that in the vicinity of critical points of magnetic configurations the standard approximations adopted to describe the plasma dynamics are no longer valid. In such regions the drift approximation, i.e., the assumption that the adiabatic invariants are constant, can no longer be applied. On the other hand, the particle spends only a finite time interval in the nonadiabatic region, since there its motion is unstable. After a finite time interval it gets out of the nonadiabatic region, and gets into the drift region as it is seen in Fig. 12b. Matching the solution described by the particle trajectories in different regions, we can describe the particle motion and hence the acceleration near critical points of the magnetic configurations.

Under the conditions of space plasmas, the radiation losses during the charged particle acceleration in the magnetic reconnection processes are caused by the backward Compton scattering and by synchrotron losses. A characteristic time of the synchrotron losses for the electron with energy \mathcal{E} is given by the expression

$$\tau_B = \frac{3m_e^4 c^7}{2e^4 B^2 \mathcal{E}}. \quad (75)$$

As it was shown in Ref. [109], during solar flares this effect limits the ultrarelativistic electron energy to a value of about several tens of GeV.

E. Electron Vortices in Collisionless Plasmas

The vortical fluid motion is well known to be widely present under the earth's and space conditions. In laser plasmas, when ultra short and high intensity EMW pulse propagates in the collisionless plasmas, it accelerates a copious number of relativistic electrons. The electric current of fast electrons produces quasistatic magnetic field, whose evolution results in the formation of electron vortex structures. They naturally take a form of the vortex rows [111], as it is shown in the LHS inset to Fig.13. A strong magnetic field in the relativistic laser plasma has been detected experimentally [112].

The interacting vortices can be described within the framework of a two-dimensional

theoretical model. By taking \mathbf{B} to be along the z -axis ($\mathbf{B} = B\mathbf{e}_z$), and assuming all the quantities to depend on the x, y -coordinates, we obtain from vector equations (72) one equation

$$\partial_t(\Delta B - B) + \{B, (\Delta B - B)\} = 0 \quad (76)$$

for a scalar function $B(x, y, t)$. Here

$$\{f, g\} = \partial_x f \partial_y g - \partial_x g \partial_y f \quad (77)$$

are the Poisson brackets. Equation (76) is known as the Charney equation [113] or the Hasegawa-Mima (HM) [114] equation in the limit of zero drift velocity. In this case linear perturbations with the dispersion equation $\omega = |\mathbf{k}|(\mathbf{k} \cdot \mathbf{B}_0)/(1 + k^2)$ correspond to the Rossby waves, the drift waves or to the whistler waves, respectively.

Equation (76) has a discrete vortex solution, for which the generalized vorticity is localized at the points $\mathbf{x} = \mathbf{x}^\alpha$:

$$\Omega = \Delta B - B = \sum_{\alpha} \kappa_{\alpha} \delta(\mathbf{x} - \mathbf{x}^{\alpha}(t)). \quad (78)$$

Solving this equation we find that the magnetic field is a superposition of the magnetic fields created at isolated vortices localized at the coordinates $\mathbf{x}^{\alpha}(t)$: $B = \sum_{\alpha} B^{\alpha}$ with

$$B^{\alpha}(\mathbf{x}, \mathbf{x}^{\alpha}(t)) = -\frac{\kappa_{\alpha}}{2\pi} K_0(|\mathbf{x} - \mathbf{x}^{\alpha}(t)|). \quad (79)$$

Here and below $K_n(\xi)$ are modified Bessel functions.

The curves $\mathbf{x}^{\alpha}(t)$ are determined by the characteristics of equation (76). The characteristic equations have the Hamiltonian form

$$\kappa_{\alpha} \dot{x}_i^{\alpha} = J_{ij} \frac{\partial \mathcal{H}}{\partial x_j^{\alpha}} = -\frac{1}{2\pi} J_{ij} \sum_{\beta \neq \alpha} \kappa_{\alpha} \kappa_{\beta} \frac{(x_i^{\alpha} - x_j^{\beta})}{l_{\alpha\beta}^2}, \quad (80)$$

where J_{ij} is the antisymmetric unit matrix. The Hamiltonian is given by

$$\mathcal{H} = -\sum_{\alpha < \beta} \kappa_{\alpha} \kappa_{\beta} K_0(l_{\alpha\beta})/2\pi. \quad (81)$$

In the case of the Euler hydrodynamics, a point vortex is described by $(\kappa_{\alpha}/2\pi) \ln |\mathbf{x} - \mathbf{x}^{\alpha}(t)|$, instead of the expression (79) which involves the Bessel function $K_0(|\mathbf{x} - \mathbf{x}^{\alpha}(t)|)$. The latter results in the shielding of the interaction between vortices at large distances. A typical scale length of the problem under consideration in the case of the EMHD vortex systems, is equal to the collisionless electron skin-depth, $d_e = c/\omega_{pe}$.

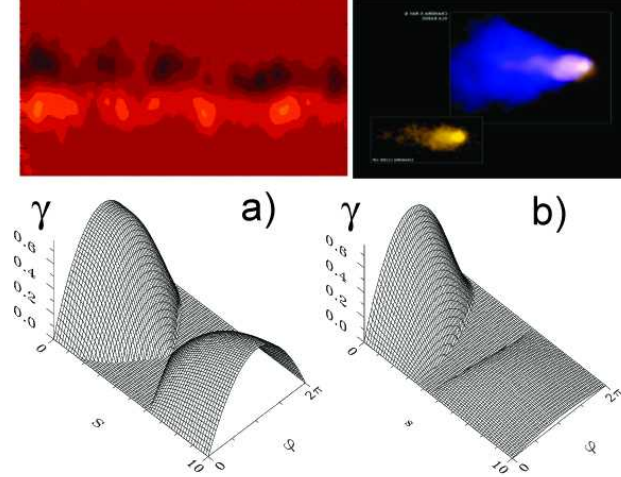


FIG. 13: Instability growth rate on s and q for the vortex row described within the framework of the Euler (a) and Hasegawa-Mima (b) approximations. Left inset: The vortex row seen in the magnetic field patch distribution in a plasma behind the laser pulse. Right inset: The Mouse pulsar (NASA/CXC/SAO, Chandra image of G359.23-0.82 pulsar)[124].

Considering the problem of the stability of an infinite vortex chain we assume that all vortices have the same absolute intensity and take. In the initial equilibrium the vortices have coordinates (Fig. (13))

In the case of an antisymmetrical vortex row with $\sigma = 1/2$, we expect a more complicated behavior of the perturbations, compared to that of the symmetrical configuration. As noted in Lamb's monograph [115], in standard hydrodynamics the antisymmetrical von Karman's vortex row is stable for $q/s \approx 0.281$, where s and q give a distance between the vortices in the unperturbed vortex row along the x and y coordinates. A dependence of the instability growth rate on s and q for the vortex row described within the framework of the Euler hydrodynamics approximation is shown in Fig. 13a.

By direct inspection of the row instability described by the Hasegawa-Mima equations we can see that for large distance between neighbouring vortices the antisymmetric vortex row is stable for

$$3s^2/4 > q > s/2. \quad (82)$$

(see Fig. 13b).

F. A Role of the Weibel Instability in the Quasistatic and Turbulent Magnetic Field Generation

The quasistatic magnetic field generation in relativistic laser plasmas occurs due to the fast electron beam interaction with the background plasma. It can be understood in terms of the Weibel instability [122] or in the generic case, in terms of the electromagnetic filamentation instability. When the fast electron beam propagates in the plasma, its electric current is compensated by the current carried by the plasma electrons. A repulsion of the oppositely directed electric currents results in the electron beam filamentation and in the generation of a strong magnetic field [125]. An electromagnetic filamentation instability leads to the generation of a quasistatic magnetic field and is associated with many small-scale current filaments [126]. Each filament consists of a direct and of a return electric current which repel each other. This produces a strong electric field, which accelerates the ions in the radial direction. In the long term evolution, the successive coalescence of the small-scale current filaments forms a large scale magnetic structure. This process is accompanied by the reconnection of the magnetic field lines, by the formation of current sheets, and by strong ion acceleration inside these sheets [127].

The filamentation phenomena are of great interest for the explanation of the quasi-static magnetic field origin in laser plasmas irradiated by relativistically strong EMW [123]. Counterstreaming electric current configurations naturally appear in space at the fronts of colliding electron-positron and electron-ion plasma clouds [128] as in the cases of the Galactic Gamma Ray Bursts and in shock waves in supernova remnants. The filamentation instability generates the magnetic field required by the theory of the synchrotron afterglow in GRB [129]. The Weibel instability has been invoked as a mechanism of the primordial magnetic field generation by colliding electron clouds in cosmological plasmas [130].

The filamentation instability developing in the vicinity of shock wave fronts together with other types of instabilities [131] plays the role of the source of strong electromagnetic turbulence invoked in the theoretical models of the Fermi acceleration of cosmic rays [132, 133]. A realization of the Fermi acceleration mechanism of Type A at the shock wave front is discussed below in Section VIII.

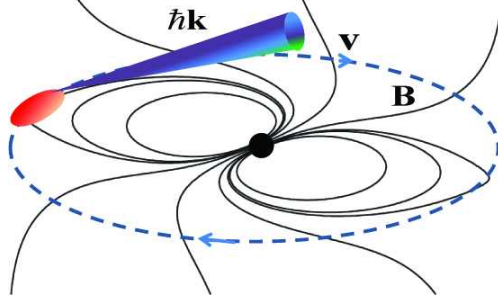


FIG. 14: Schematic pulsar magnetosphere, according to Ref. [134]. A rotating relativistic electron lump emits electromagnetic radiation by the antenna mechanism.

VII. RELATIVISTIC ROTATOR

In Ref. [134] the antenna mechanism of the pulsar radiation emission has been proposed. According to this mechanism in the pulsar magnetosphere, which is a rotating magnetic dipole, the magnetic dipole interaction with a plasma at the magnetosphere periphery induces strong modulations of the electron density, an electron density lump. The phase velocity of the electron lump can be arbitrarily close to the speed of light in vacuum. It is directed along a circle as illustrated in Fig. ?? . As a result of the curvilinear acceleration, the electron lump emits a radiation, whose properties are similar to the synchrotron radiation [135].

In the context of Relativistic Laboratory Astrophysics it is remarkable that the relativistic rotating dipole can naturally be formed in the laser plasma. Laser-plasma interactions provide an opportunity to reproduce nonlinear electrodynamics effects under astrophysical conditions in the laboratory. In Ref. [136] it is demonstrated that high-power coherent synchrotron-like radiation can be generated by the relativistic charge density wave rotating self-consistently inside an electromagnetic-dipole solitary wave, dwelling in a laser plasma. The relativistically strong laser pulse can generate relativistic EM subcycle solitary waves in a plasma [137], as it was indicated by particle-in-cell (PIC) simulations. An analytical description of solitons of this type was developed in Refs. [138]. Figure 15 presents the structure of electric and magnetic fields inside the soliton [139]. The soliton resembles an oscillating or rotating electric dipole. The toroidal magnetic field, shown in Fig. 15, indicates that, besides the strong electrostatic field, the soliton also has an electromagnetic field. The electrostatic and electromagnetic components in the soliton are of the same order of magnitude.

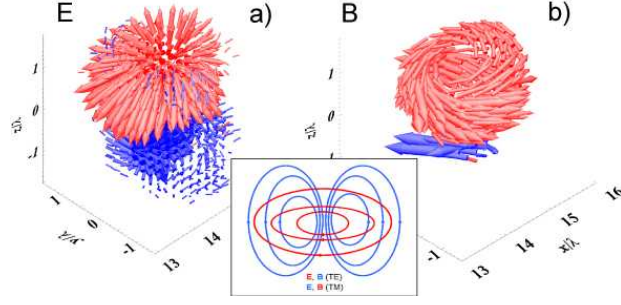


FIG. 15: Structure of electric (a) and magnetic (b) fields inside the EM relativistic soliton. Inset: The magnetic- and electric-field topology in the TE (with poloidal magnetic field and toroidal electric field) and in the TM (with poloidal electric field and toroidal magnetic field) solitons.

The 3D solitons emit high-frequency EM radiation, whose frequency is much higher than the Langmuir frequency [136]. This radiation is emanated from the electron density hump rotating in the wall of the soliton cavity, similar to coherent synchrotron-like emission. This radiation has the characteristics of a well pronounced outgoing spiral EM wave, Fig. 16 a). The emission of the spiral wave correlates to the rotation of the electron density hump in the cavity wall, and it leads to the spiral modulations of the electron density (see Fig. 16 b)). The density hump gyrates in a circle, and the period of revolution is exactly equal to the soliton period. The polarization of the spiral wave corresponds to the well known synchrotron radiation [135] and the density hump emission is coherent.

The results of 3D PIC simulations, presented in Ref. [136], distinctly demonstrated relativistic rotating dipoles excited by the circularly polarized laser pulse in an underdense plasma. The dipoles are associated with the relativistic electromagnetic solitons.

VIII. SHOCK WAVES

Phenomena taking place at shock-wave fronts play a key role in various astrophysical conditions. The characteristic dimensionless parameters that determine the shock wave propagation are the magnetic Mach number, $M_A = v_{SW}/v_A$, equal to the ratio of the shock wave front velocity, v_{SW} , to the Alfvén velocity, v_A , the ratio of the gas pressure to the magnetic pressure, $8\pi nT/B^2$, and θ , the angle between the normal to the front and the magnetic field.

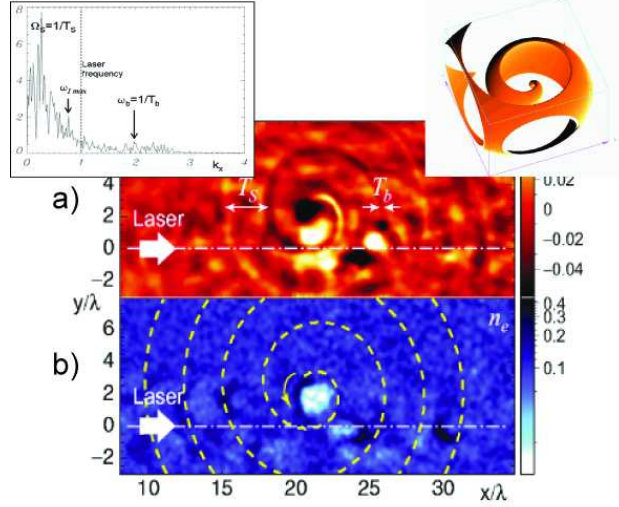


FIG. 16: a) Cross sections of the magnetic field component $eBz = m_e c$ in the plane x, y . b) The electron density distribution. Right inset: The EM field of the rotating electric charge rotating. Left inset: A frequency spectrum of the emitted EM wave.

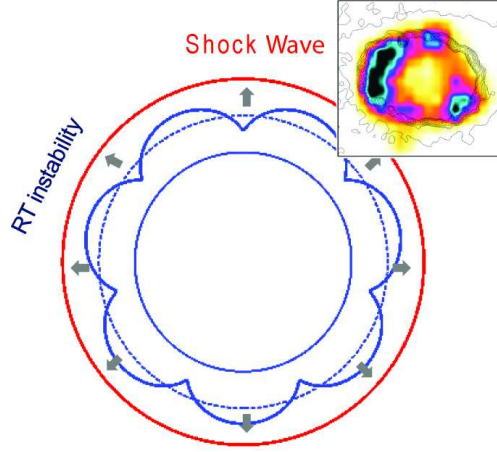


FIG. 17: Schematic view of the shock waves and contact discontinuity in a supernova remnant. In the inset: X-ray and optical image of supernova remnant SNR 1987A [148, 149].

A. Shock Waves in Supernova Remnants

The origin of cosmic rays (CR) is one of the most interesting problems in astroparticle physics [14, 142]. The observation of ultrahigh-energy cosmic rays indicates that cosmic rays exist beyond 10^{20} eV and certainly beyond 10^{19} eV energies greater than the GZK cutoff [143] for the extragalactic sources due to the pionization loss of protons that decay

by collision with cosmic microwave background photons. The galactic CR spectra in the energy range above a few GeV and below $\approx 10^7$ GeV are power-laws with the total cosmic ray spectrum being

$$I_{CR} = 1.8 \times \mathcal{E}^{-\kappa} \frac{\text{particles}}{\text{cm}^2 \text{s st GeV}} \quad (83)$$

in the energy range from a few GeV to 100 TeV with $\kappa \approx 2.7$. Around 10^{15} eV (the “knee”), the slope steepens from $\kappa \approx 2.7$ to $\kappa \approx 3$. The energies 10^{18} eV correspond to the ultra high energy cosmic rays (UHECR), which sources are associated with active galactic nuclei (AGNs) [144].

For the most advanced theoretical models of galactic cosmic ray acceleration with the energy below 10^{17} eV the shock waves formed in the supernova explosions are most important. This process is related to the nature of collisionless shock waves [131].

During explosions of type II supernovae an energy \mathcal{E}_{tot} of the order of 10^{51} erg is released. The frequency of supernova explosions is about 1/30 per year. Estimates [14] show that approximately 2% of the energy of a supernova should be transferred into the cosmic ray energy.

In the initial stage of the evolution of a supernova envelope a system of shocks is formed (17). The matter ejected from a star is decelerated and compressed in the inner shock wave. Through the circumstellar gas a second shock wave propagates. The matter ejected from a star is separated from the circumstellar gas by a contact discontinuity, which is unstable with respect to a Rayleigh-Taylor instability. The RT instability leads to the relatively long scale modulations of the gas density inside the supernova shells.

When the mass of the swept interstellar gas becomes larger than the mass ejected from the star, the propagation of outer shock in Fig. (17) is described by the Sedov-Taylor self-similar solution. The radius of the shock, R_{SW} , as a function of time is related to the energy, \mathcal{E}_{SN} , released in the explosion and to the gas density ρ_0 by the relation

$$R_{SW}(t) = 1.51 \left(\frac{\mathcal{E}_{SN}}{\rho_0} \right)^{1/5} t^{2/5} = \frac{5}{2} v_{SW} t. \quad (84)$$

The shock wave velocity, $v_{SW}(t) \approx t^{-3/5}$, decreases with time. At a later time when the radiation losses become important, the law of the supernova envelope expansion changes. The asymptotic time dependence of the SN envelope radius is given by $R_{SW}(t) \approx t^{2/7}$ (see Ref. [14] and references therein).

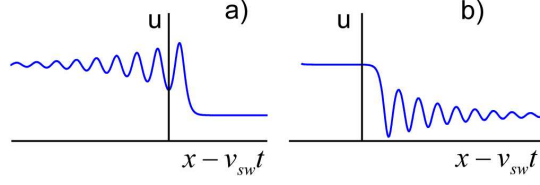


FIG. 18: Structure of collisionless shock wave front for $\beta > 0$ (a) and for $\beta < 0$ (b).

B. Collisionless Shock Waves

If the shock wave has a relatively small amplitude, $M_A < M_1 \approx 1.5$ (the precise value depends on β and θ), then the front profile is laminar in structure and it is determined by a joint action of the dispersion and dissipation on the nonlinear waves propagation. These effects are described in the framework of the Korteweg-de Vries-Burgers equation:

$$\partial_t u + u \partial_x u - \nu \partial_{xx} u + \beta \partial_{xxx} u = 0. \quad (85)$$

The stationary wave propagating with constant velocity is described by a solution, which shows the change of the amplitude of the wave from zero far ahead of the shock wave front, to $u_1 = 2v_{sw}$ far behind the shock wave front.

The decay of the oscillation amplitude, with the coefficient equal ν/β , results in the decrease of the amplitude of solitons as it is shown in Fig. 18. If dissipation effects are more important than the effects of dispersion, $\nu/\beta \gg 1$, there are no oscillations at the shock wave front. More precisely, the decay should be large enough, $\nu \gg v_{cr}$, with

$$\nu_{cr} = \sqrt{4\beta u_1}. \quad (86)$$

In this case the wave has a monotonous structure.

In the case of $\nu/\beta \ll 1$, the dispersion effects are dominant and there are many well seen solitons near the front. For $\beta > 0$ the oscillations are localized behind the front (Fig. ??a), while for $\beta < 0$ they are ahead of the front (Fig. ??b).

For example, in the case of the magnetoacoustic shock waves in a plasma, propagating almost perpendicularly to the direction of the magnetic field, the dispersion coefficient, $\beta \approx v_a c^2 / 2\omega_{pe}^2$, is positive. This means that the oscillations are localized behind the front of

the magnetoacoustic shock wave propagating perpendicularly to the magnetic field. When the direction of the magnetoacoustic wave propagation is almost parallel to the direction of the magnetic field, the coefficient $\beta \approx -v_a c^2 / 2\omega_{pi}^2$ is negative with $\omega_{pi} = \sqrt{4\pi n e^2 / m_i}$. The oscillations at the front of the magnetoacoustic shock wave, propagating quasi-parallelly with respect to the magnetic field, are localized ahead of the front.

Dissipation, which determines the distance of the oscillation decay, can be due to anomalous resistance and viscosity arising from an excitation of the plasma instability, i.e. the Weibel instability of counterpenetrating plasmas. If the amplitude of the shock wave is large, $M_A > 3$, a high level of turbulent fluctuations of electric and magnetic fields are excited ahead and behind the wave front.

In the laser-plasma physics context, the observation of collisionless shocks was reported by several authors [44], aiming to reproduce astrophysical phenomena in small scale laboratories. However, in general when the shocks were observed with optical probing techniques, the front structure could hardly be resolved. In Ref. [145] the propagation in a rarefied plasma ($n_e < 10^{15} \text{cm}^{-3}$) of collisionless shock waves being excited following the interaction of a long ($L = 470 \text{ps}$) and intense ($I = 10^{15} \text{Wcm}^{-2}$) laser pulse with solid targets, has been investigated via proton probing techniques [146]. The shocks' structures and related electric field distributions were reconstructed with high spatial and temporal resolution. The experimental results are described within the framework of the nonlinear wave description based on the Korteweg-de Vries-Burgers equation (85).

C. Diffusive Acceleration of Charged Particles at the Shock Wave Front

The charged particle interaction with fluctuations of the electric and magnetic field in a turbulent plasma may result in particle scattering and diffusion. When the shock wave propagates in a turbulent medium, an average velocity of electromagnetic fluctuations is different in the regions ahead and behind the shock front. Efficiently the particle appears to move between semitransparent (due to diffusion) walls with a decreasing distance between them. A model transport equation describing the particle convection, diffusion and acceleration has a form [14]

$$\partial_t f + \text{div}(\mathbf{u} f - D \nabla f) =$$

$$\frac{1}{p^2} \partial_p \left[p^2 \left(\frac{p}{3} \text{div } \mathbf{u} - K(p) \right) f \right], \quad (87)$$

where $f(p, x, t)$ is the fast particle distribution function, p , x and t the particle momentum, coordinate and time, v_{SW} being the speed of the shock wave propagation, and D is the diffusion coefficient. A term in the right hand side describes regular acceleration or deceleration of the charged particles:

$$\frac{dp}{dt} = -K(p) - \frac{1}{3} p \text{div } \mathbf{u}. \quad (88)$$

The function $K(p)$ corresponds to the Compton and synchrotron losses important for the cosmic ray electron component:

$$K(p) = -\beta_B c p^2 \quad (89)$$

with

$$\beta_B = 8 \times 10^{-25} \left(\frac{B^2}{8\pi} + w_{ph} \right) \frac{1}{eV \cdot s} \quad (90)$$

An average change of the particle momentum proportional to $p \text{div } \mathbf{u}$ occurs due to the particle bouncing between converging, $\text{div } \mathbf{u} < 0$, or diverging, $\text{div } \mathbf{u} > 0$, scattering centres.

The average particle bouncing between two reflecting plates with distance L as a function of time provides a simple example of a dynamic system with conservation of the longitudinal adiabatic invariant, $J_{||} = pL$ [150, 151]. The phase plane shown in the inset to Fig. 19, illustrates the Fermi acceleration mechanism of the first type (type A according to Ref. [152]). By virtue of the longitudinal adiabatic invariant conservation, for decreasing distance between the plates, $dL/dt < 0$, the particle momentum grows, i.e. the particle acquires energy.

The velocity distribution in the vicinity of the front of an infinitely thin shock wave, propagating from left to right, has the form: $u(X) = u_1$ in the region $X > 0$, and $u(X) = u_2$ for $X < 0$. Here $X = x - v_{SW}t$. The velocities ahead the shock front and behind it are related to each other as

$$u_2 = u_1 \frac{\kappa + 1}{\kappa - 1}. \quad (91)$$

Here, κ is the polytropic index. For an infinitely thin shock wave front the divergence of the velocity is equal to

$$\text{div } \mathbf{u} = (u_1 - u_2) \delta(X). \quad (92)$$

Substituting this expression into Eq. (87), we obtain that the charged particle acceleration at the fronts of collisionless shock waves propagating in a turbulent plasma is described by

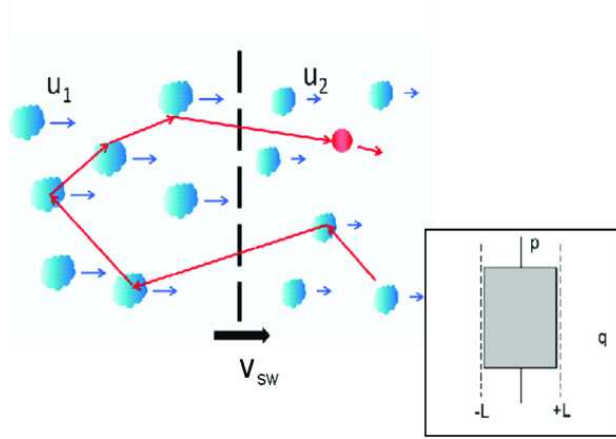


FIG. 19: Particle diffusion at the front of a shock wave propagating in a turbulent plasma. Inset: the phase plane of the particle bouncing between two plates.

the equation (see Ref. [14] and references therein)

$$\begin{aligned} \partial_X(u(X)f - D\partial_X f) + \frac{1}{p^2}\partial_p(p^2 K(p)f) = \\ - 2\frac{u_2}{3(\kappa + 1)}\delta(X)\frac{1}{p^2}\partial_p(p^3 f). \end{aligned} \quad (93)$$

In the limit, when the energy losses are negligibly small, this equation has a solution, which gives a power law dependence of the distribution function, $f \propto p^{-k}$ with the index value $k = 3u_2/(u_2 - u_1)$. For $\kappa = 5/3$ the index equals $k = 4$, i.e. $f \propto p^{-4}$, or the energy spectrum $d\mathcal{N}_{CR}(\mathcal{E})/d\mathcal{E} \propto \mathcal{E}^{-3}$ is close to the power law index observed in the galactic cosmic ray energy spectrum (see Eq. (83)).

For the cosmic ray electron component in the high energy limit, at the energy when we cannot neglect the Compton and synchrotron losses, there is a cut off in the spectrum [153]. For typical parameters in supernova remnants, $D = 10^{25}\text{cm}^2\text{s}^{-1}$, $B = 10^{-4}\text{G}$, $u_1 = 10^8\text{ cm s}^{-1}$, the radiation losses limit the energy of ultrarelativistic electrons by values of the order of 10 TeV.

Under the conditions of typical timescale of the laser plasmas the synchrotron losses of ultrarelativistic electrons interacting with the self-generated magnetic field is of the order of

$$\tau_B = 5 \left(\frac{10^3}{\gamma_e} \right) \left(\frac{10^9 \text{G}}{B} \right)^2 \text{ fs}. \quad (94)$$

IX. CONCLUSIONS

Finally, we note that the development of superintense lasers with parameters in the ELI range will provide the necessary conditions for experimental physics where it will become possible to study ultrarelativistic energy of accelerated charged particles, super high intensity EMW and the relativistic plasma dynamics. A fundamental property of the plasma to create nonlinear coherent structures, such as relativistic solitons and vortices, collisionless shock waves and high energy particle beams, and to provide the conditions for relativistic regimes of the magnetic field line reconnection, makes the area of relativistic laser plasmas attractive for modeling of processes of key importance for relativistic astrophysics.

Acknowledgement

We appreciate discussions and comments from V. S. Beskin, M. Borghesi, P. Chen, R. Diehl, A. Ya. Faenov, M. Kando, Y. Kato, T. Kawachi, J. K. Koga, K. Kondo, G. Korn, G. Mourou, N. B. Narozhny, T. A. Pikuz, A. S. Pirozhkov, N. N. Rosanov, V. I. Telnov, A. G. Zhidkov. This work was partially supported by the Ministry of Education, Science, Sports and Culture of Japan, Grant-in-Aid for Creative Scientific Research (A), 202244065, 2008.

The authors acknowledge the support by the European Commission under contract ELI pp 212105 in the framework of the program FP7 Infrastructures-2007-1.

-
- [1] M. Shriber, *Science* **310** (2005) 1610; M. Dunne, *Nature Phys.* **2** (2006) 2; J. Shambaret, *et al.*, *Quantum Electronics and Laser Sci. Conf. QETS'07* (2007) 2.
 - [2] B. Remington, D. Arnett, P. Drake, and H. Takabe, *Science* **248** (1999) 1488; P. Chen, *AAPPS Bull.* **13** (2003) 3 [ArXiv:astro-ph/03003350]; N. C. Woolsey, C. Courtois, and R. O. Dendy, *Plasma Phys. Control. Fusion* **46** (2004) B397; B. Remington, R. Drake, D. Ryutov, *Rev. Mod. Phys.* **78** (2006) 755.
 - [3] J. D. Lindl, *et al.*, *Phys. Plasmas* **11** (2004) 339.
 - [4] A. D. Strickland and G. Mourou, *Opt. Commun.* **56** (1985) 212.
 - [5] S. Weinberg, arXiv:hep-th/0511037 v1.
 - [6] A. Linde, *Particle Physics and Inflationary Cosmology* (Harwood, Chur, Switzerland, 1990).

- [7] M. Yu. Khlopov and S. G. Rubin, *Cosmological Pattern of Microphysics in the Inflationary Universe* (Kluwer, New York, 2004).
- [8] D. H. Perkins, *Particle Astrophysics* (Oxford University Press, Oxford, 2003).
- [9] F. Wilczek, International J. Mod. Phys. A, **23** (2008) 1791.
- [10] N. Kaloper and J. Terning, arxiv.org/abs/physics/0703062v2; M. Bleicher, arxiv.org/abs/physics/0703062v2.
- [11] I. Ya. Aref'eva and I. V. Volovich, arxiv.org/abs/0710.2696v2.
- [12] J. Rafelski, International J. Mod. Phys. A, **16** (2007) 813.
- [13] G. Mourou, T. Tajima, and S. V. Bulanov, Rev. Mod. Phys. **78** (2006) 309.
- [14] V. S. Berezhinskii, S. V. Bulanov, V. L. Ginzburg, V. A. Dogiel, V. S. Ptuskin, *Astrophysics of cosmic rays* (North Holland Publ. Co. Elsevier Sci. Publ. Amsterdam, 1990).
- [15] F. A. Aharonian, *et al.*, Phys. Rev. D **66** (2002) 023005; M. V. Medvedev, Phys. Rev. E **67** (2003) 045401 (R).
- [16] T. Tajima and J.M. Dawson, Phys. Rev. Lett. **43** (1979) 267.
- [17] P. Chen, J. M. Dawson, R. Huff, and T. Katsouleas, Phys. Rev. Lett. **54** (1985) 693.
- [18] P. Chen, T. Tajima, and Y. Takahashi, Phys. Rev. Lett. **89** (2002) 161101; M. Hoshino, Astrophys. J. **672** (2008) 940; J. T. Frederiksen, Astrophys. J. **680** (2008) L5; P. Chen, *et al.*, Plasma Phys. Control. Fusion **51** (2009) 024012.
- [19] T. Zh. Esirkepov, *et al.*, Phys. Rev. Lett. **92** (2004) 175003.
- [20] S. V. Bulanov, T. Zh. Esirkepov, J. Koga, and T. Tajima, Plasma Phys. Rep. **30** (2004) 196.
- [21] P. N. Lebedev, Ann. der Physik, **6** (1901) 433; A. S. Eddington, Mon. Not. Roy. Astr. Soc. **85** (1925) 408.
- [22] E. A. Milne, Mon. Not. Roy. Astr. Soc. **86** (1926) 459; S. Chandrasekhar, Mon. Not. Roy. Astr. Soc. **94** (1934) 522; N. J. Shaviv, Astrophys. J. **532** (2000) L137.
- [23] J. Arons, Astrophys. J. **388** (1992) 561; C. F. Gammie, Mon. Not. Roy. Astr. Soc. **297** (1998) 929; M. C. Begelman, Astrophys. J. **551** (2001) 897.
- [24] V. I. Veksler, Atomic Energy **2** (1957) 427.
- [25] S. V. Bulanov, *et al.*, Nucl. Instrum. Methods Phys. Res. A **540** (2005) 25.
- [26] S. S. Bulanov, *et al.*, Phys. Rev. E **78**, (2008) 026412.
- [27] T. V. Liseykina, M. Borghesi, A. Macchi, and S. Tuveri, Plasma Phys. Control. Fusion **50** (2008) 124033; A. P. L. Robinson, *et al.*, New J. Phys. **10** (2008) 013021.

- [28] P. Goldreich, Phys. Scripta **17** (1978) 225; T. Piran, Astrophys. J. **257** (1982) L23.
- [29] S. V. Bulanov, T. Zh. Esirkepov, and T. Tajima, Phys. Rev. Lett. **91** (2003) 085001.
- [30] M. Bordag, U. Mohideen, and V.M. Mostepanenko, Phys. Rep. **353** (2001) 1; A. M. Fedotov, Yu. E. Lozovik, N. B. Narozhny, and A. N. Petrosyan, Phys. Rev. A **74** (2006) 013806.
- [31] W. G. Unruh, Phys. Rev. D **14** (1976) 870; P. Chen and T. Tajima, Phys. Rev. Lett. **83** (1999) 256; R. Schutzhold, G. Schaller, and D. Habs, Phys. Rev. Lett. **97** (2006) 121302; L. Crispino, *et al.*, Rev. Mod. Phys. **80** (2008) 787.
- [32] N. N. Rosanov, JETP **76** (1993) 991; N. N. Rosanov, JETP **86** (1998) 284.
- [33] J. J. Klein and B. P. Nigam, Phys. Rev. **135**, B1279 (1964); J. Lundin, *et al.*, Phys.Rev. A **74** (2006) 043821; D. Tommasini, *et al.*, arXiv:0802.0101v1 [physics.optics].
- [34] A. M. Fedotov and N. B. Narozhny, Physics Letters A **362** (2007) 1.
- [35] A. Di Piazza, A. I. Milstein, and C. H. Keitel Phys. Rev. A **76** (2007) 032103; A. Di Piazza, K. Z. Hatsagortsyan, and C. H. Keitel, Phys.Rev. A **78** (2008) 062109.
- [36] M. Marklund and P. Shukla, Rev. Mod. Phys. **78** (2006) 591.
- [37] Y. I. Salamin, S. X. Hu, K. Z. Hatsagortsyan, and C. H. Keitel, Phys. Reports **427** (2006) 41.
- [38] J. Schwinger, Phys. Rev. **82** (1951) 664.
- [39] V. B. Beresteskii, E. M. Lifshitz, and L. P. Pitaevskii, *Quantum Electrodynamics* (Pergamon, New York, 1982).
- [40] K. Birkeland, *The Norwegian Aurora Polaris Expedition, 1902-1903* (Aschenhoug & Co. Christiania, 1908).
- [41] H. Alfven and C.-G. Falthammar, *Cosmic Electrodynamics* (Oxford, 1963); T. Tajima and K. Shibata *Plasma Astrophysics* (Addison-Wesley, Reading, 1997).
- [42] V. E. Fortov, Physics - Uspekhi **50** (2007) 347.
- [43] P. J. Baum and A. Bratenahl, Adv. Electronics and Electron Phys. **54** (1980) 1; S. V. Bulanov, I. Ya. Butov, Yu. S. Gvaladze, A. M. Zaborov, A. N. Kuzyutin, M. A. Ol'shanetskij, R. G. Salukvadze, B. D. Tsurtsumija, Sov. J. Plasma Phys. **12**, 180 (1986); S. V. Bulanov and A. G. Frank, Sov. J. Plasma Phys. **18** (1992) 1535; R. L. Stenzel, *et al.*, Phys. Plasmas **9** (2002) 1925; J. Egedal, *et al.*, Phys. Rev. Lett. **90** (2003) 135003; A. G. Frank, *et al.*, Phys. Plasmas **12** (2005) 052316; M. Yamada, *et al.*, Phys. Plasmas **14** (2007) 058102.
- [44] D. W. Koopman and D. A. Tidman, Phys. Rev. Lett. **18** (1967) 533; A. R. Bell *et al.*, Phys.

- Rev. A **38** (1988) 1363; N. C. Woolsey, *et al.*, Phys. Plasmas **8** (2001) 2439.
- [45] Yu. P. Zakharov, *et al.*, Journal of Physics: Conf. Series **112** (2008) 042011.
- [46] L. I. Sedov, *Similarity and dimensional methods in mechanics* (New York, Academic Press, 1959); G. I. Barenblatt, *Scaling, Self-similarity, and Intermediate Asymptotics: Dimensional Analysis and Intermediate Asymptotics* (Cambridge, Cambridge University Press, 1996).
- [47] I. M. Podgorny and R. Z. Sagdeev, Sov. Phys. Uspekhi **98** (1970) 445.
- [48] C.-G. Falthammar, Space Sci. Rev. **15** (1974) 803.
- [49] S. V. Bulanov, Plasma Phys. Control. Fusion **48** (2006) B29.
- [50] F. Pegoraro, T. Zh. Esirkepov, and S. V. Bulanov, Physics Letters A **347** (2005) 133.
- [51] L. V. Keldysh, Sov. Phys. JETP **20** (1965) 1307.
- [52] P. Corkum, Phys. Rev. Lett. **71** (1993) 1994.
- [53] L. D. Landau and E. M. Lifshitz, *The Classical Theory of Fields* (Pergamon Press, Oxford, 1980).
- [54] A. I. Akhiezer and R. V. Polovin, Sov. Phys. JETP **30** (1956) 915.
- [55] S.-W. Bahk, *et al.*, Opt. Lett. **29** (2004) 2837; V. Yanovsky, *et al.*, Opt. Express **16** (2008) 2109.
- [56] G. S. Bisnovaty-Kogan, Ya. B. Zel'dovich, and R. A. Syunyaev, Sov. Astron. J. **15** (1971) 17; S. Wilks, *et al.*, Astrophys. Space. Sci. **298** (2005) 347.
- [57] I. Kuznetsova, D. Habs, and J. Rafelski, Phys. Rev. D. **78** (2008) 014027.
- [58] C. Gahn, *et al.*, Appl. Phys. Lett. **77** (2000) 2662.
- [59] Ya. B. Zeldovich and A. F. Illarionov, Sov. Phys. JETP **34** (1972) 467; A. D. Steiger and C. H. Woods, Phys. Rev. D **5** (1972) 2912; Ya. B. Zel'dovich, Sov. Phys. Uspekhi **18** (1975) 79; C. H. Keitel, *et al.*, J. Phys. B: At. Mol. Opt. Phys. **31** (1998) L75; A. G. Zhidkov, *et al.*, Phys. Rev. Lett. **88** (2002) 185002; J. K. Koga, T. Zh. Esirkepov, and S. V. Bulanov, Phys. Plasmas **12** (2005) 093106; J. Koga, T. Z. Esirkepov, and S. V. Bulanov, J. Plasma Phys. **72** (2006) 1315; V. I. Berezhiani, S. Mahajan, and Z. Yoshida, Phys. Rev. E. **78** (2008) 066403; A. Di Piazza, Lett. Math. Phys. **83** (2008) 305.
- [60] A. R. Bell and J. G. Kirk, Phys. Rev. Lett. **101** (2008) 200403.
- [61] W. Dittrich and H. Gies, *Probing the Quantum Vacuum: Perturbative Effective Action Approach in Quantum Electrodynamics and Its Applications* (Springer, Berlin, 2000).
- [62] V. S. Popov, Phys. At. Nuclei **68**, 686 (2005).

- [63] N. B. Narozhnyi, S. S. Bulanov, V. D. Mur, and V. S. Popov, JETP Lett. **80** (2004) 382.
- [64] S. S. Bulanov, A. M. Fedotov, and F. Pegoraro, Phys. Rev. **71** (2005) 016404; R. Ruffini, *et al.*, Phys. Lett. A **371** (2007) 399.
- [65] N. B. Narozhnyi, *et al.*, Phys. Lett. A **330** (2004) 1.
- [66] C. Bamber, *et al.*, Phys. Rev. D **60** (1999) 092004.
- [67] E. Loetstedt, *et al.*, Phys. Rev. Lett. **101** (2008) 203001.
- [68] V. S. Beskin, A. V. Gurevich, and Ya. N. Istomin, *Physics of the Pulsar Magnetosphere* (Cambridge Univ. Press, Cambridge, 1993).
- [69] A. Gruzinov, Phys. Rev. Lett. **94** (2005) 021101.
- [70] J. Gunn and J. Ostriker, Phys. Rev. Lett. **22** (1969) 728.
- [71] J. Hester, Ann. Rev. Astron. Astrophys. **46** (2008) 127.
- [72] D. Clowe, *et al.*, Astrophys. J. **648** (2006) L109.
- [73] S. Humphries, Jr., *Charged Particle Beams* (Wiley, New York, 1990).
- [74] T. Zh. Esirkepov, Y. Kato, and S. V. Bulanov, Phys. Rev. Lett. **101** (2008).
- [75] M. Kando, *et al.*, in: 1st International Symposium Laser-Driven Relativistic Plasmas Applied for Science, Industry, and Medicine// eds. S. V. Bulanov, H. Daido. AIP Conf. Proc. **1024** (2008) 197.
- [76] S. V. Bulanov, *et al.*, Phys. Plasmas **12** (2005) 073103.
- [77] S. V. Bulanov and T. Tajima, J. Particle Accelerator Society of Japan **2** (2005) 35; T. Zh. Esirkepov, *et al.*, Phys. Rev. Lett. **96** (2006) 014803.
- [78] M. Kando, *et al.*, JETP **105** (2007) 916.
- [79] P. Michel, *et al.*, Phys. Rev. E **74** (2006) 026501; I. Y. Dodin and N. J. Fisch, Phys. Plasmas **15** (2008) 103105.
- [80] M. Borghesi, *et al.*, Fus. Sci. Technology, **49** (2006) 412; M. Borghesi, *et al.*, Plasma Phys. Control. Fusion, **50** (2008) 124040.
- [81] S. V. Bulanov and V. S. Khoroshkov, Plasma Phys. Rep. **28** (2002) 453.
- [82] T. Zh. Esirkepov, *et al.*, Phys. Rev. Lett. **89** (2002) 175003; S. V. Bulanov, *et al.*, Plasma Phys. Rep. **28** (2002) 975; A.P.L Robinson and P. Gibbon, Phys. Rev. E **75** (2007) 015401(R); T. Morita, *et al.*, Phys. Rev. Lett. **100** (2008) 145001.
- [83] C. Schwoerer, *et al.*, Nature **439** (2006) 445.
- [84] A. V. Gurevich, *et al.*, Sov. Phys. JETP **22** (1966) 449; E. G. Gamalii and R. Dragila, *Kratk.*

- Soobshch. Fiz. AN SSSR **2** (1988) 16; S. V. Bulanov, L. M. Kovrizhnykh, and A. S. Sakharov, Phys. Rep. **186** (1990) 1; P. Mora, Phys. Rev. Lett. **90** (2003) 185002.
- [85] Y. Kishimoto, K. Mima, T. Watanabe, and K. Nishikawa, Phys. Fluids **26** (1983) 2308; F. Mako and T. Tajima, Phys. Fluids **27** (1984) 1815.
- [86] S. V. Bulanov, *et al.*, Plasma Phys. Rep. **30** (2004) 21.
- [87] F. Pegoraro and S.V. Bulanov, Phys. Rev. Lett. **99** (2007) 065002.
- [88] E. Ott, Phys. Rev. Lett. **29** (1972) 1429; W. Manheimer, *et al.*, Phys. Fluids **27** (1984) 2164; F. Pegoraro, *et al.*, Phys. Rev. E **64** (2001) 016415.
- [89] S. Kar, *et al.*, Phys. Rev. Lett. **100** (2008) 225004; M. Borghesi, *et al.*, Plasma Phys. Control. Fusion **50** (2008) 124040.
- [90] C. W. Misner, K. Thorn, J. A. Wheeler, *Gravitation* (Freeman, San Francisco, 1973); S. Weinberg, *Gravitation and Cosmology: Principles and Applications of the General Theory of Relativity* (Wiley, New York, 1973)
- [91] N. Arkani-Hamed, S. Dimopoulos, and G. Dvali, Phys. Lett. B **429** (1998) 263.
- [92] F. R. Arutyunian and V. A. Tumanian, Phys. Lett. **4** (1963) 176; Y. Li, *et. al.*, Phys. Rev. ST Accel. Beams **5** (2002) 044701.
- [93] N. M. Naumova, J. A. Nees, I. V. Sokolov, B. Hou, and G. A. Mourou, Phys. Rev. Lett. **92** (2004) 063902; N. M. Naumova, J. Nees, and G. Mourou, Phys. Plasmas **12** (2005) 056707; A. Isanin, *et al.*, Phys. Lett. A **337** (2005) 107; S. S. Bulanov, T. Z. Esirkepov, F. F. Kamenets, and F. Pegoraro, Phys. Rev. E **73** (2006) 036408; N. M. Naumova, *et al.*, New J. Phys. **10** (2008) 025022; V. V. Kulagin, *et al.*, Phys. Plasmas **14** (2007) 113101; N. N. Rosanov, JETP Lett. **88** (2008) 577; D. Habs, M. Hegelish, *et al.*, Appl Phys B **93** (2008) 349354; H.- C. Wu and J. Meyer-ter-Vehn, arXiv:0812.0703v1 [physics.plasm-ph] 3 Dec 2008; J. Meyer-ter-Vehn and H. - C. Wu, arXiv:0812.0710v1 [physics.plasm-ph] 3 Dec 2008; T. Zh. Esirkepov, *et al.*, arXiv:0812.0401v1 [physics.plasm-ph] 2 Dec 2008.
- [94] K. Landecker, Phys. Rev. **86** (1952) 852; V. L. Granatstein *et al.*, Phys. Rev. A **14** (1976) 1194; J. A. Pasour, V. L. Granatstein, and R. K. Parker, *ibid.* **16** (1977) 2441.
- [95] V. I. Semenova, Sov. Radiophys. Quantum Electron. **10** (1967) 599; W. B. Mori, Phys. Rev. A **44** (1991) 5118; R. L. Savage, Jr., *et al.*, Phys. Rev. Lett. **68** (1992) 946.
- [96] A. Einstein, Ann. Phys. (Leipzig) **17** (1905) 891; W. Pauli, *Theory of Relativity* (Pergamon, New York, 1958).

- [97] A. V. Panchenko, *et al.*, Phys. Rev. E **78** (2008) 056402.
- [98] S. V. Bulanov and A. S. Sakharov, JETP Lett. **54** (1991) 203; S. V. Bulanov, F. Pegoraro, and A. M. Pukhov, Phys. Rev. Lett. **74** (1995) 710; N. H. Matlis, *et al.*, Nature Phys. **2** (2006) 749.
- [99] M. Kando, *et al.*, Phys. Rev. Lett. **99** (2007) 135001; A.S. Pirozhkov, *et al.*, Phys. Plasmas **14** (2007) 080904; M. Kando, *et al.*, :0705.0872v1 [physics.plasm-ph] 2007.
- [100] W. Heisenberg and H. Euler, Z. Phys. **98** (1936) 714.
- [101] S. V. Bulanov and P. V. Sasorov, Soviet Astronomy J. **19** (1976) 464; S. V. Bulanov and F. Cap, Soviet Astronomy J. **32** (1988) 436; J. Buchner and L. M. Zelenyi, J. Geophys. Res. **94** (1989) 11821; D. L. Vainshtein, L. M. Zelenyi, and A. I. Neishtadt, Plasma Physics Reports, **21** (1995) 484; J. F. Drake, M. Swisdak, H. Che and M. A. Shay, Nature **443** (2006) 553; S. Zenitani and M. Hoshino, Astrophys. J. **670** (2007) 702 [arXiv:0708.1000v2]; Y. Lyubarsky and M. Liverts, Astrophys. J. **682** (2008) 1436.
- [102] S. I. Syrovatskii, Ann. Rev. Astron. Astrophys. **19** (1981) 163; 1; S. I. Syrovatskii, S. V. Bulanov, V. A. Dogiel, in: *Scientific Reviews E, Astrophysics and Space Physics Reviews*, vol. 2 (North Holl. Publ. Co, Amsterdam, 1983) p. 385
- [103] D. Biskamp, *Magnetic Reconnection in Plasmas* (Cambridge Univ. Press, Cambridge, 2000).
- [104] G. A. Askar'yan, *et al.*, Comm. Plasma Phys. Controlled Fusion **17** (1995) 35.
- [105] P. M. Nilson, *et al.*, Phys. Rev. Lett. **97** (2006) 255001; C. K. Li, *et al.*, Phys. Rev. Lett. **99** (2007) 055001; P. M. Nilson, *et al.*, Phys. Plasmas **15** (2008) 092701.
- [106] P. A. Sweet, in *Electromagnetic Phenomena in Cosmic Physics./ Ed. by B. Lehnert*. (Cambridge University Press, 1958) p. 122.
- [107] E. Parker, *Cosmical Magnetic Fields: their origin and their activity* (Oxford University Press, New York, 1979).
- [108] S. V. Bulanov, *et al.*, Phys. Lett. A **203** (1995) 219.
- [109] S. V. Bulanov, *et al.*, Sov. Astronomy. Lett. **11** (1985) 159.
- [110] S. V. Bulanov, *et al.*, in: *Reviews of Plasma Physics*, vol. 22 // edited by V. D. Shafranov, (Kluwer Academic / Plenum Publishers, New York, 2001), p. 227.
- [111] S. V. Bulanov, M. Lontano, T. Zh. Esirkepov, F. Pegoraro, and A. M. Pukhov, Phys. Rev. Lett. **76** (1996) 3562.
- [112] M. Borghesi, *et al.*, Phys. Rev Lett. **80** (1998) 5137; M. Tatarakis, *et al.*, Nature (London)

- 415** (2002) 280..
- [113] G. K. Batchelor, *Introduction to Fluid Mechanics* (Cambridge University Press, Cambridge, 1973).
 - [114] A. Hasegawa and K. Mima, Phys. Rev. Lett. **39** (1977) 205.
 - [115] H. Lamb, *Hydrodynamics* (Cambridge University Press, Cambridge, 1932).
 - [116] A. S. Kingsep, K. V. Chukbar, and V. V. Yan'kov, in: *Reviews of Plasma Physics*, vol. 16 // Ed. by B. B. Kadomtsev (Consultants Bureau, New York, 1990) p. 243.
 - [117] S. V. Bulanov, F. Pegoraro, and A. S. Sakharov, Phys. Fluids B **4** (1992) 2499; K. Avinash, et al., Phys. Plasmas **5** (1998) 2946; P. A. Cassak, et al., Phys. Rev. Lett. **98** (2007) 215001.
 - [118] H. P. Furth, I. Killen, and M. N. Rosenbluth, Phys. Fluids **6** (1963) 459; B. Coppi, G. Laval, and R. Pellat, Phys. Rev. Lett. **16** (1966) 1207.
 - [119] S. V. Basova, et al., Sov. J. Plasma Phys. **17** (1991) 615.
 - [120] A. Fruchtman and H. R. Strauss, Phys. Fluids B **5** (1993) 1408; M. Hosseinpour, et al., Phys. Plasmas **16** (2009) 012104.
 - [121] J. W. Dungey, Phil. Mag. Ser. 7. **44** (1953) 725.
 - [122] E. S. Weibel, Phys. Rev. Lett **2** (1959) 83.
 - [123] V. Yu. Bychenkov, et al., Sov. Phys. JETP **71** (1990) 709; G. A. Askar'yan, et al., JETP Lett. **60** (1994) 251.
 - [124] B. M. Gaensler, et al., Astrophys. J. **616** (2004) 383.
 - [125] F. Califano, F. Pegoraro, and S. V. Bulanov, Phys. Rev. E **56** (1997) 963.
 - [126] M. Honda, J. Meyer-ter-Vehn, and A. M. Pukhov, Phys. Plasmas **7** (2000) 1302.
 - [127] J. I. Sakai, et al., Phys. Plasmas **9** (2002) 2959.
 - [128] Y. Kazimura, J.-I. Sakai, T. Neubert, and S. V. Bulanov, Astrophys. J. **498** (1998) L183.
 - [129] M. V. Medvedev and A. Loeb, Astrophys. J. **526** (1999) 697.
 - [130] J. I. Sakai, R. Schlickeiser, and P. Shukla, Phys. Lett. A **330** (2004) 384.
 - [131] D. A. Tidman and N. A. Krall, *Shock Waves in Collisionless Plasmas* (Wiley-Interscience, New York, 1971); T. M. O'Neil and F. V. Coroniti, Rev. Mod. Phys. **71** (1999) 404.
 - [132] L. O. Silva, et al., Astrophys. J. **596** (2003) L121.
 - [133] H. Takabe, et al., Plasma Phys. Control. Fusion **50** (2008) 124057.
 - [134] V. L. Ginzburg and V. V. Zheleznyakov, Ann. Rev. Astron. Astrophys. **13** (1975) 511.
 - [135] V. L. Ginzburg, *Applications of Electrodynamics in Theoretical Physics and Astrophysics*

- (Gordon and Breach, New York, 1989).
- [136] T. Zh. Esirkepov, *et al.*, Phys. Rev. Lett. **92** (2004) 255001.
 - [137] S. V. Bulanov, *et al.*, Phys. Fluids B **4** (1992) 1935; S. V. Bulanov, *et al.*, Phys. Rev. Lett. **82** (1999) 3440.
 - [138] V. A. Kozlov, A. G. Litvak, and E. V. Suvorov, Sov. Phys. JETP **49** (1979) 75; P. K. Kaw, A. Sen, and T. Katsouleas, Phys. Rev. Lett. **68** (1992) 3172; T. Zh. Esirkepov, *et al.*, JETP Lett. **68** (1998) 36; D. Farina and S. V. Bulanov, Phys. Rev. Lett. **86** (2001) 5289.
 - [139] T. Esirkepov, *et al.*, Phys. Rev. Lett. **89** (2002) 275002.
 - [140] N. M. Naumova, *et al.*, Phys. Rev. Lett. **87** (2001) 185004.
 - [141] M. Borghesi, *et al.*, Phys. Rev. Lett. **88** (2002) 135002.
 - [142] M. Kachelries, arXiv:0801.4376v1 [astro-ph] 29 Jan 2008.
 - [143] K. Greisen, Phys. Rev. Lett. **16** (1966) 748; G. T. Zatsepin and V. A. Kuz'min, Sov. Phys. JETP. Lett. **4** (1966) 78.
 - [144] J. Abraham (Pier Auger Collaboration) Science **318** (2007) 938.
 - [145] L. Romagnani, *et al.*, Phys. Rev. Lett. **101** (2008) 025004.
 - [146] M. Borghesi, *et al.*, Phys. Plasmas **9** (2002) 2214.
 - [147] G. F. Krymskii, Sov. Phys.–Dokl. **23** (1977); W. I. Axford, E. Leer and G. Skadron, Proc. 15th Int. Cosmic Ray Conf. (Plovdiv) **11** (1977) 132; A. R. Bell, Mon. Not. Roy. Astr. Soc. **182** (1978) 147; R. D. Blandford and J. P. Ostriker, Astrophys. J. **221** (1978) 29; S. V. Bulanov and I. V. Sokolov, Soviet Astronomy J. **28** (1984) 515; M. A. Malkov and L. O. Drury, Rep. Prog. Phys. **64** (2001) 429.
 - [148] D. Burrows, *et al.*, Astrophys. J. **543** (2000) L149.
 - [149] V. S. Imshennik and D. K. Nadezhin, Usp. Fiz. Nauk, **158** (1988) 561; V. S. Imshennik and D. K. Nadezhin, in: *Sov. Sci. Rev. E Astrophysics and Space Physics Reviews*, vol. 8 (North Holl. Publ. Co, Amsterdam, 1983) p. 1.
 - [150] A. Lichtenberg and M. Liberman, *Regular and stochastic dynamics* (Wiley, New York, 1984).
 - [151] S. V. Bulanov, *Introduction to Nonlinear Physics* (Scuola Normale Superiore, Pisa, 2000).
 - [152] E. Fermi, Phys. Rev. **75** (1949) 1169; Astrophys. J. **119** (1954) 1.
 - [153] S. V. Bulanov and V. A. Dogiel, Sov. Astron. J. Lett. **5** (1979) 521.